DEPARTMENT OF PHYSICS

TECHNISCHE UNIVERSITÄT MÜNCHEN

Master's Thesis in Physics

A Theory of Photoconductive Sampling of Optical Fields in Atomic Gases

Manoram Agarwal

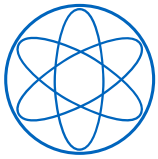

DEPARTMENT OF PHYSICS

TECHNISCHE UNIVERSITÄT MÜNCHEN

Master's Thesis in Physics

A Theory of Photoconductive Sampling of Optical Fields in Atomic Gases

Eine Theorie über die Abtastung optischer Felder in atomaren Gasen durch deren ultraschnelle Leitfähigkeitsänderungen

Author:	Manoram Agarwal
Supervisor:	Prof. Dr. David Egger
Advisor:	Prof. Dr. Vladislav S. Yakovlev
Submission Date:	19.08.2022

I confirm that this master's thesis in physics is my own work and I have documented all sources and material used.

Garching, 19.08.2022 Manoram Agarwal

Abstract

When a high-intensity optical field impinges on an atom, it ionizes it [1]. The rate of this ionization depends on the exact time-evolution of the optical field. However, in quantum mechanics, a precise determination of the time-dependent strong-field ionization probability is non-trivial. Its definition and the resulting predictions change with the theoretical models. Photoconductive sampling [2] is a measurement technique that uses a short photoionization event to resolve optical fields with a sub-femtosecond resolution. It facilitates insights into ultrafast dynamics like those of an electron. In photoconductive sampling, the light-matter interaction can be modeled as a classical Newtonian acceleration of an electron that is set free in the presence of the optical field that is to be measured, i.e., sampled. However, in the case of strong-field ionization, this classical description requires using an ionization rate model with all its ambiguities. Fortunately, the technique's measured quantity can be mapped to a quantum mechanical observable. In this work I obtain a quantum mechanical description for photoconductive sampling that circumvents the ambiguity present in the definition of an ionization rate. I solve the time-dependent Schrödinger equation (TDSE) analytically by making what is known as the strong field approximation (SFA) [3]. The results from the analytical expressions are then compared with the results of another ab initio TDSE solver that does not use SFA. My results provide a definition of ionization rate that is exact and unambiguous within the context of photoconductive sampling. Comparisons with the TDSE solver indicate that the excited bound states of the hydrogen atom play a more active role in strong-field ionization than was previously believed. Of special experimental relevance is the finding that, for strong-field ionization, reducing the central wavelength of the optical pulse improves the technique's time resolution. Additionally, for the same central wavelength, lower intensities result in shorter ionization-durations, albeit with diminishing returns. This trend reverses beyond a certain point.

Contents

1. Introduction

Sixty ticks of a clock make a minute. That single tick occurs because a quartz crystal resonator oscillates 32768 times to count a second [4]. One such oscillation takes only about 30 micro-seconds [5]. Further down the scale are the atomic and molecular interactions causing this and they last only a few picoseconds. One might assume that it is possible to continue going to ever shorter time scales, however, the journey naturally concludes at attosecond— the scale at which quantum mechanics occurs. This is the timescale at which all electron dynamics can be resolved. Beyond this one would get into the dynamics within the nucleus, which are not as important in determining electronic and chemical properties of a medium. By resolving dynamic behavior of the electrons, one hopes to better understand the underlying fundamental physics. Eventually, this knowledge might be useful to control electronics with that speed. A future where electronics can be clocked at a petahertz [6] is indeed very enticing.

The study of physical dynamics at attosecond time scale is called attosecond metrology. It started in 2001 with the ability to produce sub-femtosecond light pulses [7] to create a measurement technique called attosecond streaking [8, 9]. Since then, physicists have invented several other techniques capable of attosecond metrology— TIPTOE [10–12], mid-infrared electro-optic sampling [13, 14], and photoconductive sampling [15–17] to name a few.

The focus of this thesis is photoconductive sampling. It is a technique that exploits photoconductivity— a medium's ability to become conductive when a photon impinges on it [18]— to resolve the electric field of a light pulse. One may model photoconductive sampling in the following manner: the injection pulse abruptly makes the material photoconductive. While photoconductivity is changing, i.e., during the time that the injection pulse is photoinjecting charge carriers, the drive pulse accelerates these free charges. This changes the charges' momentum distribution whose cumulative effect is a drift current unique to the exact time evolution of the drive pulse. The drift current can be picked up by the metal electrodes, either directly due to the free charges reaching them or via mirroring.

By delaying the arrival time of the drive pulse, the moment during which injection occurs can be controlled to sample distinct parts of the drive pulse, yielding a delay-dependent drift current. For a sufficiently weak drive pulse, its vector potential and

the measured delay-dependent drift current is linearly related:

$$S_{\mathrm{d}}(\omega) = A_{\mathrm{drive}}(\omega) G^{\star}(\omega),$$

where ω is the angular frequency, S_{d} the drift current, A_{drive} the vector potential of the drive pulse, and G a response function that is purely determined by the medium and the injection pulse. The drift current is an experimental observable and

$$S_{\mathrm{d}} = -e\, N \left\langle \mathbf{p} \cdot \hat{\mathbf{e}}_{\mathrm{drive}} \right\rangle ,$$

where e is the elementary charge, N the number of ionized atoms, $\hat{\mathbf{e}}_{\mathrm{drive}}$ the polarization direction of the drive field, and $\mathbf{p}$ the momentum of the free charge carrier—a quantum mechanical observable.
To model this classically, one needs to know the rate at which the injection pulse creates free charge carriers in the medium. Finding the ionization rate is non-trivial and its definition varies with the models used. For the same material and injection pulse, the predicted ionization rates vary with the models. Moreover, the models are only valid for a limited domain of an optical pulse's central wavelengths and intensities [19–22].
The problem that plagues the definition of ionization rate combined with the fact that we do have a quantum mechanical observable that perfectly explains photoconductive sampling motivated the central hypothesis of this thesis:

> The delay dependence of the residual electric current, which is a measurable physical observable, may contain sufficient information to retrieve the ionization rate from quantum calculations, thus reconciling the quantum and classical models of photoconductive sampling.

Based on this central idea, I aim to achieve the following:

1. Using the strong field approximation (SFA) [3, 19, 23], derive an analytical solution for the delay-dependent drift current.

2. Comparing the classical and quantum mechanical description of photoconductive sampling , define a quantum mechanical ionization rate that accurately describes photoconductive sampling.

3. Computing the ionization rate for a variety of pulses, find how to best optimize photoconductive sampling for the highest time resolution.

4. Compare the SFA results with an ab initio solution of the time-dependent Schrödinger equation.

I have divided this thesis into three larger parts with the aim to save a prospective reader's time.

Part I explains all the concepts that are used in the rest of this thesis. None of it is my original work and only paraphrased from my perspective. chapter 2 defines the quantities used to quantify an optical pulse and its interaction with a medium. chapter 3 introduces the strong field approximation, a method to analytically solve the time-dependent Schrödinger equation. chapter 4 describes how photoconductive sampling works. chapter 5 contains a brief overview of two other techniques that are also used for attosecond meteorology, attosecond streaking and TIPTOE. chapter 6 contains the theoretical background of the TDSE solver that I use to benchmark my own results against. I have prioritized brevity over clarity as all the topics discussed already have excellent reviews. Rather than describing all the details, I selectively mention information most relevant for the thesis.

Part II contains a lot of detailed calculations that use the well-known results of chapter 3 to obtain analytical expressions of the quantities I am interested in. chapter 7 contains the derivation of the delay-dependent drift current. chapter 8 shows how the analytical expression of the delay-dependent drift current can be reformulated to reconcile the quantum mechanical expression with its classical counterpart. I personally find it very enlightening as a few simple transformations lead to equations with a form that strongly support the original hypothesis that motivated this thesis. chapter 9 contains the analytical expressions computed specifically for the hydrogen atom and chapter 10 summarizes all the approximations that were involved in obtaining the analytical expressions.

Part III contains all numerical results for the hydrogen atom obtained by solving the equations mentioned in part II. chapter 11 and chapter 12 present the results for the two sub-types of photoconductive sampling. For benchmarking, chapter 12 also contains plots comparing the predictions made by my analytical theory and the predictions of an ab initio TDSE solver that does not make the approximations used in the former. Finally, chapter 13 summarizes the conclusion made in the previous chapter and has some additional remarks to invigorate further discussions.

Part I.

Preliminaries

2. Basic Definitions

2.1. Light

Based on Maxwell's equation [24], a **light wave** is defined as an electromagnetic wave that propagates in the direction $\mathbf{k}$ at the speed of light c in vacuum, with electric and magnetic fields, $\mathbf{E}(t)$ and $\mathbf{B}(t)$, given by

$$\begin{aligned}\mathbf{E}(t) &= -\nabla\phi(t) - \frac{\partial \mathbf{A}(t)}{\partial t},\\ \mathbf{B}(t) &= \nabla \times \mathbf{A}(t).\end{aligned}$$

Here, $\mathbf{A}$ and ϕ are the vector and scalar potentials that are not unique, such that potentials

$$\begin{aligned}\mathbf{A}' &\coloneqq \mathbf{A} + \nabla\psi\\ \phi' &\coloneqq \phi - \frac{\partial\psi}{\partial t}\end{aligned}$$

also result in the same electromagnetic fields. This freedom in choice of the scalar and vector potentials is an example of **gauge freedom**. Formulating the Hamiltonian of a system requires an explicit or an implicit gauge choice. However, fixing the gauge should not change the observable physical reality [25] and the choice is often a matter of mathematical convenience.
In vacuum, $\mathbf{E} \perp \mathbf{B} \perp \mathbf{k}$. A light wave is **linearly polarized** if its electric field is confined within a single plane, the **polarization** direction, along the direction of propagation.
Introductory texts often limit discussions of light-matter interaction to a light wave of a specific frequency. Such an object does not have a beginning or an end in time. A **light pulse** on the other hand is a wave packet—a superposition of light waves of multiple frequencies and intensities. A pulse has a finite width both in time and frequency domains. The term 'optical field' also refers to a light pulse and it helps distinguish the effects of the electromagnetic field of light from any other field.
A light pulse can be arbitrarily complicated and quantifying it requires simultaneous knowledge of both its spectrum, and its time dependent phase. Techniques such as the one being investigated within this thesis facilitate such measurements. My aim is

not an exact simulation of the laboratory conditions. I want to gain useful physical insights. Idealized conditions are better for that. For my numerical simulations, I use pulses whose electric field can be defined mathematically as:

$$\mathbf{E}(t) = E_0 \frac{\xi(t)e^{i(\omega_0 t+\eta)} + \xi^\star(t)e^{-i(\omega_0 t+\eta)}}{2}\hat{e}, \tag{2.1}$$

where $\hat{e}$ is the polarization direction, E_0 the maximum electric field, $\xi(t)$ the pulse envelope or the envelope function, η the carrier-envelope phase, and $\omega_0 = \frac{c}{2\pi\lambda_0}$ the central angular frequency of the carrier wave. The intensity of such a pulse is:

$$I_0 = \frac{c\epsilon_0 E_0^2}{2}.$$

The choice of envelope function is not as important so long as it does not cause spurious ionization due to moments of sudden turn-off and turn-on of the optical field. In simulations, the envelop function is often defined for the integral of the electric field, rather than the field directly as this ensures that the integral of the field over the entire pulse duration is zero. If this condition were violated, any electron that was free before the arrival of an optical field would gain a nonzero momentum due to the interaction with this field. This should not occur in the non-relativistic regime. I use the 'cos8' pulse envelope [26],

$$\xi_{\cos 8}(t) \coloneqq \cos^8\left(2\arccos\left(2^{-1/16}\right)\frac{t}{\tau_{\mathrm{FWHM}}}\right).$$

Here, τ_{FWHM} defines the width of the envelope function at half maximum. The actual pulse duration can be modulated with this.
The carrier-envelope phase defines the alignment between the maxima of the envelope and the wave. The two extreme cases are the 'cosine' and the 'sine' pulses shown in Figure 2.1. I define intensity in watts per centimeter squared (W cm^{-2}), wavelength in nanometers (nm), and FWHM using either femtoseconds (fs) or optical cycles (OptCyc). An optical cycle defines the time it takes for a laser of a given frequency to complete one cycle, i.e., a complete back and forth. It is used to quantify the number of oscillations the defined laser pulse makes.

2.2. Ponderomotive Energy and Keldysh Parameter

The average kinetic energy with which a free electron would quiver due to the acceleration by the optical electric field $\mathbf{E}(t)$ is called ponderomotive energy. It is

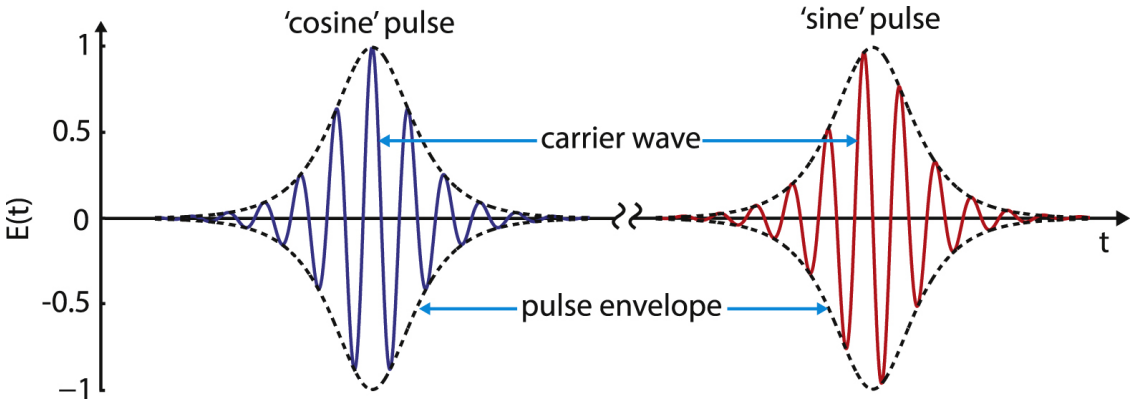

Figure 2.1.: Visualization of a light pulse defined using a central frequency and an envelope function. The 'cosine' and the 'sine' pulses represent CEPs where the wave is in phase and out of phase respectively [27]

given by

$$U_\mathrm{p} = \frac{e^2 E_0^2}{4 m_\mathrm{e} \omega_0^2} = \frac{2e^2}{c \epsilon_0 m_\mathrm{e}} \frac{I}{4\omega_0} \overset{\text{au}}{=} \frac{E_0^2}{4\omega_0}. \tag{2.2}$$

Here, ϵ_0 is the vacuum permittivity, c the speed of light, e the electron charge, and m_e its mass. Using atomic units (au) corresponds to setting $e = m_\mathrm{e} = \hbar = a_0 = 1$, $\epsilon_0 = 1/4\pi$, $\alpha c = 1$, and $\alpha \approx 1/137$.
To quantify the strength of the optical field relative to the medium, knowledge of the energy needed to create a free electron, the binding energy, is necessary. For the hydrogen atom,

$$E_\mathrm{bind} \coloneqq E_\mathrm{ion.} \coloneqq W_\mathrm{b} = 13.6 \text{ eV} \overset{\text{au}}{=} 0.5 \text{ au}.$$

The relation between the photon energy, the frequency, and the wavelength allows defining the light pulse with respect to a central wavelength, frequency, or photon energy interchangeably- according to the quantity most relevant for the discussion.

$$E_\nu = h\nu = \frac{hc}{\lambda} = \hbar\omega. \tag{2.3}$$

In atomic units, the photon energy is the same as its angular frequency.
With this I can also define a convenient dimensionless quantity to compare the binding energy and the ponderomotive potential—the Keldysh parameter

$$\gamma_\mathrm{K} = \sqrt{\frac{W_\mathrm{b}}{2U_\mathrm{p}}} = \frac{c\sqrt{2mW_\mathrm{b}}}{2\pi\lambda e E_0}. \tag{2.4}$$

The Keldysh parameter compares the strength with which a free electron would oscillate inside an optical field to that of the strength with which an electron is bound to the atom.

2.3. Dipole Approximation

For the field strengths and wavelengths that are typically used in photoconductive sampling, the spatial variance of the optical field can be neglected within the region occupied by the electron's wavefunction. It is called the dipole approximation and it is valid if,

1. The wavelength of the optical field is large compared to both the extension of the relevant bound electron states, and the maximal excursion distance of a free electron during the light-matter interaction.

2. The magnetic field of light negligibly influences electron motion, which implies that the velocities of charged particles must be nonrelativistic.

Making the dipole approximation implies that

$$\begin{aligned} &\mathbf{A}(\mathbf{r}, t) \approx \mathbf{A}(t) \\ \implies &\mathbf{B} = \nabla \times \mathbf{A} \approx 0 \end{aligned}$$

3. The Strong-Field Ionization

3.1. Phenomenological Perspective of Strong-Field Ionization

In physics, cases close to the upper and lower limits of a phenomenon are often the quite instructive. These cases might not be the ones achievable in laboratories, but they are especially useful for explaining the observed reality using digestible pieces of information. It is also nice because even the most complicated theoretical equations can be simplified under limits. As first demonstrated by Keldysh [19] the nature of strong-field light-matter interactions and thereby their limiting cases are determined by three things: the binding potential, W_b, the photon energy, and the ponderomotive energy, U_p.
With this preamble, I am in a position of defining the extremities of light matter interactions in question: $U_\mathrm{p} \ll W_\mathrm{b}$ ($\gamma_\mathrm{K} \to \infty$) and its complement. When $U_\mathrm{p} \ll W_\mathrm{b}$, ionization occurs via electron-photon interaction. On the other hand, when $U_\mathrm{p} \gg W_\mathrm{b}$, the electric field of the light pulse is so strong that ionization would occur primarily due to the electrons tunneling out of the binding potential, which gets extremely skewed (Figure 3.1) under the effect of the optical field.
"$U_\mathrm{p} \gg W_\mathrm{b}$ " is not a very precise quantification for a "strong" field. It only defines limits, and I certainly should not use these to define two distinct regimes of light-matter interactions. To remedy that, I would like to present a theoretical model and define the two extremes of ionization processes, tunneling ionization and multi-photon ionization, based on the validity of that theoretical model.

3.1.1. Quasi-Static Tunneling Ionization

For a moment let us forget about optical fields. Consider a simple DC electric field acting on a medium. For hydrogen atom, an external DC field will lower the Coulomb potential barrier. Although the electron still does not have enough energy to exit the atom classically, it can now tunnel through the lower barrier as portrayed in Figure 3.1 The stronger the applied DC field is, the more suppressed the Coulomb potential gets and the more likely ionization via tunneling becomes. Landau examined this problem for the hydrogen atom [29] and found that for DC

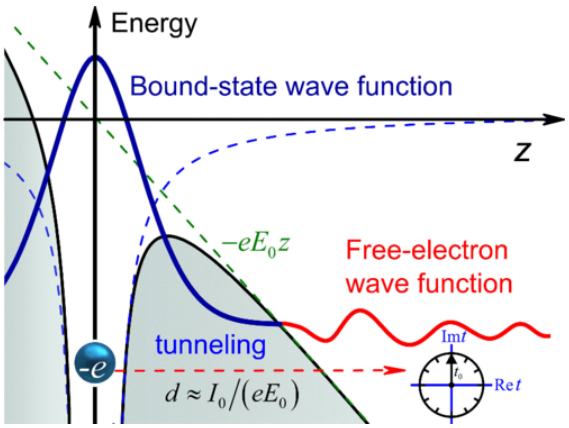

Figure 3.1.: A schematic representation of how an electric field 'skews' the Coulombic potential to allow bound electrons to tunnel out. Taken from [28]

field E, the ionization rate w is

$$\Gamma_{\mathrm{DC}} = \frac{8W_\mathrm{b}}{\hbar}\frac{W_\mathrm{b}/a_0}{|eE|}\exp\left[-\frac{4}{3}\frac{W_\mathrm{b}/a_0}{|eE|}\right] \overset{\text{au}}{=} \frac{4}{|E|}\exp\left[-\frac{2}{3}\frac{1}{|E|}\right].$$

From this result, one can quantify the characteristic field of tunneling ionization: $E_{\mathrm{tunn}} = \frac{2W_\mathrm{b}}{ea_0}$. As this is such a simple and intuitive expression, an extension to alternating electric fields, like the ones of the optical pulses, would be particularly useful. Making this jump is not very straightforward as perturbation theory is only applicable for weak fields. The initial piece in this puzzle was published by Keldysh [19], which I will discuss in section 3.2. Right now, I only want to define the term tunneling ionization within the confine of this thesis.
Under certain conditions, it is possible to treat an AC field ionization as if it were from the DC field. What this implies is that the instantaneous ionization rate is entirely defined by the absolute value of the electric field at that instant. This is referred to as the quasi-static approximation. Because the ionization rate does not depend on the frequency of light, such an ionization event cannot be interpreted as the absorption of a certain number of photons and is treated as a tunneling ionization event. An example of the quasi-static tunneling rate is given by the Ammosov, Delone, Krainov (ADK) formula [20].

$$\begin{aligned}\Gamma_{\mathrm{ADK}}(E) = C^2_{\mathrm{n}^\star,\mathrm{l}}\, f(l,m)|W_\mathrm{b}|\left(\frac{2^{5/2}}{E}|W_\mathrm{b}|^{3/2}\right)^{2n^\star-|m|-1} \\ \times\sqrt{\frac{3E}{\pi(2W_\mathrm{b})^{3/2}}}\exp\left(-\frac{2}{3}\frac{(2|W_\mathrm{b}|)^{3/2}}{E}\right)\end{aligned} \tag{3.1}$$

The factors $n^\star, C_{n^\star l}, f(l,m)$ are effective factors that allow extending the formula to more complex atoms.
Keldysh's formula for quasi-static ionization rate for the ground state hydrogen is slightly different and defines ionization as a transition from the ground state to a Volkov state. Elaborated upon later, here, it suffices to know that the Volkov state represents a free charge in an electromagnetic field.

$$\Gamma^{1s}_{\mathrm{Kel}}(E) = \frac{\sqrt{6\pi}}{2^{5/4}} W_b \left(\frac{E}{(2W_b)^{3/2}}\right)^{1/2} \exp\left(-\frac{2}{3}\frac{(2W_b)^{3/2}}{E}\right) \tag{3.2}$$

In this thesis, whenever the tunneling regime or tunneling ionization is mentioned, I am referring to field strengths where the quasi-static approach is still valid. Usually, it is when the Keldysh parameter γ_K is less than half. However, I would like to emphasize that it is not the Keldysh parameter but the validity of quasi-static limit that I use to define the tunneling regime .

3.1.2. Multi-Photon Ionization

For field strengths that are far weaker than the limit at which the quasi-static ionization model becomes invalid, one lands in the regime of multi-photon ionization. It derives its name from the fact that in this domain the ionization rate should scale as [19]

$$\Gamma_{\mathrm{MPI}} \propto E_0^{2\left(\left\lfloor \frac{W_b}{\hbar\omega} \right\rfloor + 1\right)}. \tag{3.3}$$

i.e., the ionization rate is proportional to the electric field to the power of twice the number of photons required to overcome the ionization potential. This is a significant departure from the exponential $e^{2/3E}$ dependence of the tunneling regime. I define pure multi-photon ionization regime as one where Equation 3.3 is valid.

3.1.3. Everything in Between

Having strict definitions of multi-photon ionization and tunneling ionization leaves a large domain of wavelength-intensity combinations, where neither of the ionization regimes is valid. As the two processes were the result of inspecting the limiting cases of an analytical formalism, the best way to study domains where neither of the two simplifications works is to look at the original formalism itself—the strong field approximation. I call this the intermediate regime. For an ionization rate model that is valid in this regime, it might be possible to crudely explain the observations made by considering a simultaneous multi-photon interaction and Coulomb barrier suppression. This is a helpful visualization but, the actual explanation of strong-field

ionization in the intermediate regime is the analytical expression itself— irrespective of its complicated form. If necessary, one may try identifying the two phenomena within the expression, providing mathematical support to an intuitive argument.

3.2. Strong Field Approximation

The strong-field approximation (SFA) describes an approach to solving the time dependent Schrödinger equation (TDSE) for an electron that escapes from a medium's binding potential due to interaction with a strong electromagnetic field. First popularized by the Soviet physicist Leonid Keldysh [19], it is still widely used by theoreticians working in strong field laser physics owing to its simplicity and its capability of providing phenomenological insights. It qualitatively describes most of the physics involved in strong-field ionization, and the community is aware of the processes not encapsulated in this model. Thus, it serves as a springboard to contextualize the results obtained from an experiment, both numerical and physical. Crudely, SFA may be understood as a perturbative solution. The electron starts in the ground state and is excited by the strong field. While conventional perturbation theory considers the amplitude of an optical field's oscillations to be negligible, Keldysh's approach considers fields that are strong enough to neglect the Coulomb potential's influence on a free electron. When the average photon energy of the optical field is smaller than the ionization potential, Keldysh's approach assumes that a ground state electron directly transitions to a continuum state that is free from any Coulombic influence and is only modulated by the electromagnetic field. Thus, the continuum state can be approximately modeled as a Volkov state. The Volkov states are the solution of a Hamiltonian describing a particle with charge q and mass m that experiences the electromagnetic field of light wave. They may be obtained either by solving the Klein-Gordon or the Dirac equations. There is some ambiguity with respect to the exact equation whose solution is being referred to when the Volkov Solution is mentioned. Here, I explicitly mean the non-relativistic limit. I refer the reader to existing literature [30] for the explicit relativistic solution and a discussion about important properties like completeness and orthogonality. The assumption that the electromagnetic field is so strong that the Coulomb potential may be completely ignored is what gives the strong-field approximation its name. There are far too many review articles discussing the strong-field approximation at length. For a detailed review, I would refer the reader to [31]. For this thesis, the briefer review article [32] contains all relevant information. Prioritizing brevity over completeness, I will selectively summarize SFA, presenting the equations that are the most relevant for this thesis.

3.3. Obtaining the Time-Dependent Continuum-States

My final aim is to obtain an analytical expression for the delay-dependent drift current described in chapter 4. It can be mapped to the expectation value of the momentum of the free electron in the direction of the drive field. To obtain the analytical form for any expectation value, I first need an analytical formula for the time-dependent continuum wavefunction, that is, the wave function of the ionized electron as a function of time. This section deals with the derivation of this wavefunction using SFA. Everything is in atomic units so $e = \hbar = m_e = 1$
The time dependent Schrödinger equation is given by:

$$i\frac{\partial}{\partial t}\left|\Psi\right\rangle = \hat{H}(t)\left|\Psi\right\rangle. \tag{3.4}$$

The time evolution of an initial state $\left|\Psi(0)\right\rangle$ is given by

$$\left|\Psi(t)\right\rangle = \hat{T}e^{-i\int_0^t dt'\hat{H}(t'))}\left|\Psi(0)\right\rangle, \tag{3.5}$$

where $\left|\Psi(0)\right\rangle \coloneqq \left|\phi_0\right\rangle$ is the ground state of the system. The Hamiltonian relevant for me has a combination of the Coulombic potential and the potential of the electromagnetic waves. There are numerical methods to solve this entire Schrödinger's equation. For example, I use an open-source package, tRecX (chapter 6), to do that. However, I aim to have some useful analytical expressions and for that, some form of simplification is needed. A Hamiltonian frequently contains a part, for which Equation 3.4 has a known analytical solution. Then a perturbative approach can be used to find an approximation solution of the TDSE for the entire Hamiltonian.
If the interaction with the electromagnetic waves were ignored for a second, there would only be the static potential to deal with. For atomic Hydrogen, exact solutions [33] are known. For other media, many methods exist to obtain good approximations . For example, in solids, Kohn-Sham's density functional theory (DFT) [34] can be used to obtain the energy band structure.
If the static binding potential were absent but an external electromagnetic field were present, the TDSE would have had the well-known Volkov solution which describes a free charged particle oscillating in the field.
Thus, the problem of a charged particle within a binding potential and that of a free-charged particle within an optical field are independently solvable. Bifurcating the actual Hamiltonian to reflect this should be a good start.

$$\hat{H}(t) = \hat{H}_0 + \hat{V}_L(t),$$

$\hat{H}_0$ is the unperturbed Hamiltonian of the atom and can directly act on the initial ground state. $\hat{V}_L(t) = -\mathbf{d}\cdot\mathbf{E}(t)$ expresses the interaction with the electromagnetic

pulse in length gauge, where $\mathbf{d}$ is the dipole moment of the system, and $\mathbf{E}$(t) is the the electric field strength at time t. Treating $\hat{V}_{\mathrm{L}}(t)$ as the interaction term, I obtain

$$|\Psi(t)\rangle = -i \int_0^t dt' e^{-i\int_{t'}^t \hat{H}(t'')dt''} \hat{V}_{\mathrm{L}}(t') e^{-i\int_0^{t'} \hat{H}_0 dt''} |\phi_0\rangle + e^{-i\int_0^t \hat{H}_0 dt''} |\phi_0\rangle \,, \tag{3.6}$$

which is an exact solution for such a Hamiltonian, as can be checked by substituting it in Equation 3.4. The time ordering is now implicit with $\hat{H}(t)$. This is done only for brevity. The second term on the right-hand side reflects the fact that the electron is initially in the ground state.
I am interested in free charge carriers, that is, projection onto the continuum. When projecting the final time dependent state on some continuum state with momentum $\mathbf{p}$, the second term in Equation 3.6 will drop out as there cannot be any overlap between the unperturbed ground state and the continuum.

$$|\Psi_{\mathbf{p}}(t)\rangle = -i \int_0^t dt' \, |\Psi_{\mathbf{p},\mathrm{t}}\rangle \langle \Psi_{\mathbf{p},\mathrm{t}}| \, e^{-i\int_{t'}^t \hat{H}(t'')dt''} \hat{V}_{\mathrm{L}}(t') e^{-i\int_0^{t'} \hat{H}_0 dt''} |\phi_0\rangle \,, \tag{3.7}$$

where $\Psi_{\mathbf{p},\mathrm{t}}$ represents the exact continuum state corresponding to momentum $\mathbf{p}$ at time t. So far, everything was exact, and I only managed to make a more ominous equation. The continuum state that I projected everything onto is not even a plane wave and is assumed to be some general function of unknown form. This can be simplified by using SFA, i.e., all effects of the Coulomb potential are ignored once a charge-carrier is in the continuum, only the optical fields matter. Since the Volkov solution is exact for a free charge-carrier in an optical field, the primary assumption of SFA implies that

$$e^{i\int_{t'}^t \hat{H}(t'')dt''} |\Psi_{\mathbf{p},\mathrm{t}}\rangle \approx e^{i\int_{t'}^t \hat{H}_{\mathrm{optical}}(t'')dt''} |\Psi_{\mathbf{p},\mathrm{t}}\rangle \mapsto \left|\Psi_{\mathbf{p}}^{\mathrm{Volkov}}(t')\right\rangle$$

In the coordinate space,

$$|\mathbf{r}\rangle \left\langle \mathbf{r}\middle|\Psi_{\mathbf{p}}^{\mathrm{Volkov}}(t')\right\rangle = \frac{1}{2\pi^{3/2}} \exp\left(i\mathbf{p}(t')\cdot\mathbf{r} + \frac{i}{2}\int_{\mathrm{t}}^{\infty} dt'' \mathbf{p}^2(t'') \right)$$

Within the dipole approximation I can ignore the magnetic field of an electromagnetic pulse. The scalar potential free electric field is $\mathbf{E}(t) = -\frac{\partial \mathbf{A}}{\partial t}$. Thus,

$$\mathbf{A}(t) \coloneqq \int_{\mathrm{t}}^{\infty} dt' \mathbf{E}(t').$$

If the initial momentum $\mathbf{p}_\mathrm{i}$ is known, momentum $\mathbf{p}(t_\mathrm{f})$ can be calculated using classical equations of motion [35]:

$$\begin{aligned}\mathbf{p}(t_\mathrm{f}) &= \mathbf{p}_\mathrm{i} + \int_{t_\mathrm{i}}^{t_\mathrm{f}} dt' \mathbf{a}(t') \\ &= \mathbf{p}_\mathrm{i} - \int_{t_\mathrm{i}}^{t_\mathrm{f}} dt' \mathbf{E}(t') \\ &= \mathbf{p}_\mathrm{i} - (\mathbf{A}(t_\mathrm{i}) - \mathbf{A}(t_\mathrm{f})).\end{aligned}$$

The conserved quantity $\mathbf{P} \coloneqq \mathbf{p}(t_\mathrm{f}) + \mathbf{A}(t_\mathrm{f})$ is called the canonical momentum. In terms of the momentum measured after all optical fields have completely vanished, which will be the same as the canonical momentum, the above equation can be rewritten as

$$\begin{aligned}\mathbf{p}_\mathrm{i} &= \mathbf{p}(t_\mathrm{f} \to \infty) + \mathbf{A}(t_\mathrm{i}) - \mathbf{A}(t_\mathrm{f} \to \infty) = \mathbf{p} + \mathbf{A}(t_\mathrm{i}) \\ \implies \mathbf{p}(t') &= \mathbf{p}_\mathrm{i} - (\mathbf{A}(t_\mathrm{i}) - \mathbf{A}(t')) = \mathbf{p} + \mathbf{A}(t')\end{aligned}$$

This definition allows using plane-waves instead of the abstract representation of the continuum states. For the hydrogen atom,

$$\hat{H}_0 \left|\phi_0\right\rangle = -W_\mathrm{b} \left|\phi_0\right\rangle ,$$

and using the dipole approximation,

$$\hat{V}_\mathrm{L}(t) = \mathbf{d} \cdot \mathbf{E}(t) \text{ in length guage.}$$

With all this Equation 3.7 gets simplified to:

$$\begin{aligned}\left|\Psi(\mathbf{p})\right\rangle = -i \left|\mathbf{p}\right\rangle \int_0^\infty dt' e^{-\frac{i}{2}\int_{t'}^{\infty}[\mathbf{p}+\mathbf{A}(t'')]^2 dt''} e^{+iW_\mathrm{b}t'} \\ \left\langle \mathbf{p} + \mathbf{A}(t') \right| \mathbf{d} \cdot \mathbf{E}(t') \left|\phi_0\right\rangle\end{aligned} \tag{3.8}$$

This is the wave function of an electron excited from the ground state to a state with the final momentum $\mathbf{p}$ with which all expectation values in the continuum can be calculated.

4. Resolving Optical Fields with Photoconductive Sampling

4.1. Origins of Photoconductive Sampling

Given sufficient intensity and photon energy, light pulses modify the electron distribution inside a material, changing its electronic properties. In 1975, D.H. Auston used this fact to create an extremely fast optical switch, the Auston switch [36]. Using picosecond optical pulses to change the electrical properties of a Pockel's cell— a Pockel's effect [37] based electro-optic crystal in which the light phase can be modulated by applying an electric voltage— he demonstrated the ability to switch electric signals with picosecond time precision. It has since led to an entire class of electronic devices, opto-electronics, which exploit photon-electron interaction inside solids to detect and control light [38].
In his demonstration, D.H. Auston measured the electrical conductivity across a silicon substrate. The bias across the substrate was set to 20 volts. Two pulses with central wavelengths of 1.06 micrometers and 0.53 micrometers were focused on a gap on the substrate. While the 0.53 micrometer pulse increased the conductivity at the surface, the 1.06 micrometer pulse penetrated deep enough to short the circuit by connecting it to the ground, breaking the flow of current. The delay between the two pulses could be controlled, allowing fast, user-defined switching of the semiconductor device. This is shown in Figure 4.1, taken directly from Auston's original work. The first part is the schematic representation, the second being the case where the 1.06 micrometer pulse is not present to switch off the circuit, and third which clearly demonstrates the fast switching. The speed of this switch is only limited by the speed at which the electrons inside the material respond to light pulses. If the second pulse comes before any charge carriers could be created, the switch fails.

The Auston switch successfully applies two concepts. First, light pulses modify the medium's electronic properties momentarily. Second, the knowledge of the physical change caused in the medium by a second pulse allows finer grained control in time. Photoconductive sampling is an extension and a generalization of the idea behind the Auston switch. Rather than a simple on/off state, the current is measured.

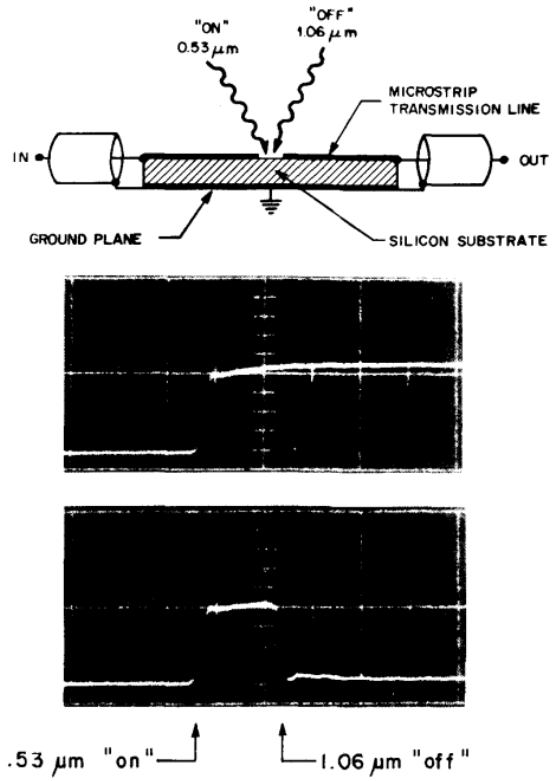

Figure 4.1.: The Auston switch in action as demonstrated by D.H Auston [36]. The measurement shows the change in surface conductivity as 0.53 µm and 1.06 µm pulses impinge on the substrate (Horizontal scale: 3 nsec/div)

Furthermore, instead of creating a fast gate using two light pulses, the technique flips the idea at its head for field sampling one of those light pulses. The fact that light pulses have similar effects on atoms and molecules adds even more flexibility in medium choices.
In the subsequent sections, I will further elaborate on photoconductive sampling as used in the context of attosecond field resolution. The idea is the same: one light pulse allows charge conduction; the second pulse modifies it. Note that an attosecond is much shorter than a picosecond, so the exact physics that allows such measurements is quite different from its picosecond counterpart.

4.2. Extending Photoconductive Sampling to Attoseconds

Within the context of this thesis, photoconductive sampling refers to a technique being developed in the Laboratory for Attosecond Physics at the Max Planck Institute of Quantum Optics. Its primary goal is achieving sub-femtosecond resolution of optical fields with a simpler experimental setup.
Resolving events in time requires an event that is even shorter than the subject of interest. As a practical example, consider a sports photographer trying shoot an athlete in action. If the shutter of his camera cannot shut fast enough, he will only capture a blurry mess. This is a fundamental restriction and cannot be circumvented. A similar restriction exists in frequency domain— the Nyquist's condition [39]. It states that to resolve a signal by sampling it at regular intervals, the sampling rate should be at least twice that of the highest frequency component in the signal. That is, sampling at least twice as many times per unit of time as the event repeating the most during that period.
Resolving fast dynamics of a system necessitates an event that is even faster and well controlled. Electron dynamics occur within a few femtoseconds. Thus, measuring how an electron-wave-packet evolves in time equates to generating 'something' that is occurring at a shorter timescale— the attosecond scale. For example, this 'something' could be the capability of attosecond pulse generation [7].
Using the ability to generate attosecond pulses, the first technique that could resolve physics occurring at attosecond scales, named attosecond streaking, was developed. From its theoretical conception [40] to its initial experimental realization [7], the technology has matured a lot. It facilitates regular measurements as well as control of dynamics occurring at these time scales. The review article by Krausz and Ivanov [41] provides an overview of the past achievements and prospects of this technology. In the context of sub-femtosecond field resolution technologies, attosecond streaking vastly predates photoconductive sampling. As I will discuss later, it was developed to overcome some of the limitations of attosecond streaking.

4.3. Photoconductive Sampling

The name, photoconductive sampling, summarizes a three-step process.
First, light pulse creates or **photo-injects** charge carriers inside a medium within a femtosecond [42]. We call the light pulse used for this the **injection pulse**.
Second, the now conductive medium interacts with **another** light pulse that is **orthogonally polarized** to the injection one; this pulse **redistributes** the charge

carrier in momentum space by accelerating them in its polarization direction. Once all optical pulses have passed the medium, the free charge carriers may have a net non-zero **drift** velocity. This second optical pulse causing the charge drift is named the **drive pulse**. The field of the drive pulse cannot inject charge carriers by itself. **Third**, one measures how the electric current flowing between the electrodes through an external electric circuit depends on the delay between the injection and drive pulses. This measured current is believed to be a function of the net charge-carrier-drift at the end of the pulses. The drive pulse, unable to excite by itself, only separates the positive and negative charge carriers in its polarization direction. The dipole created by this spatial separation of the charges induces a screened charge at the electrodes [43], which makes some charge enter the external circuit. The injection pulse creates electrons within a short time. By delaying the relative arrival time between the two pulses, one can change the part of the drive field during which the free charge carriers are available. Thus, the drift current changes with the delay and **sampling** the results for many such time-delays, a **delay scan**, yields the **delay-dependent drift current**, which, as will be explained later, is a linear function of the vector potential of the drive pulse
For more context, I present Figure 4.2. Gold electrodes are attached to the medium, crystalline quartz, to detect the current. $E_{\mathrm{i}}(t)$ refers to the injection pulse and $E_{\mathrm{d}}(t)$ refers to the orthogonal drive pulse. The electrodes are placed such that only the current parallel to E_{d} would be detected. The energy bands illustrate how the injection pulse acts upon such medium. Since most of this thesis focuses on atomic ionization, this example is also useful to show how knowledge gained from the atomic simulations could be applicable for solids by slightly modifying the concept of 'free charge'. The same experiment was also done in silicon dioxide [42]

4.3.1. Classical Interpretation

I examine the case of photoionization in hydrogen to present a classical formulation of photoconductive sampling. One ignores the spatial variance of the optical pulses under the so-called dipole approximation (see chapter 2). I use atomic units.
Given the injection field $\mathbf{E}_{\mathrm{inj}}(t)$, the ionization rate $\Gamma_{\mathrm{ion}}(t)$ gives the number of free electrons ionized by the pulse between times t and $t + dt$. Finding Γ_{ion} is not trivial but for a moment, let's just assume that it was known exactly. The drive field $\mathbf{E}_{\mathrm{d}}(t)$, designed to be incapable of free electron creation, accelerates the electrons created by the injection pulse.
After time t_{f}, when all optical pulses have completely passed the atom, an electron that became free at time t_{i} with an initial velocity $\mathbf{v}_0(t_{\mathrm{i}})$ will experience an

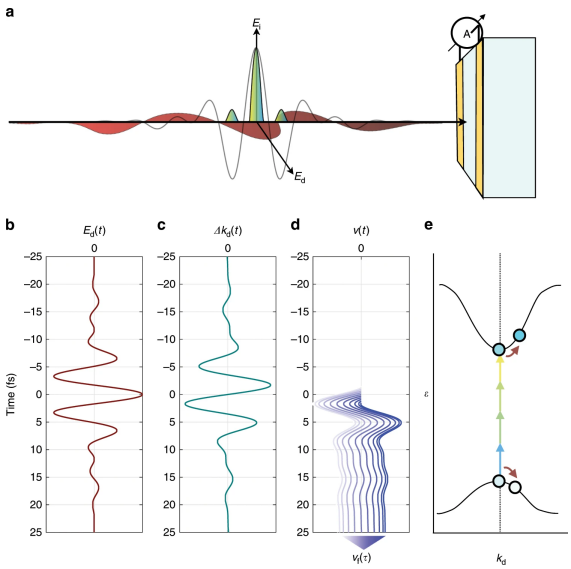

Figure 4.2.: Schematic representation of photoconductive sampling performed in crystalline quartz. In the setup **a** the injection field E_i creates electron-hole pairs (e blue-green arrows) that are then accelerated by the drive field E_d (e brown arrows). E_d shown in **b** should change the crystal momentum by an offset $\Delta k_\mathrm{d}(t)$ (**c**) that is equal to the integral of E_d. The offset determines the group velocities v(t) (**d**). Changing the time of injection by delaying the E_i by τ will yield different final group velocities such one gets $\Delta k_\mathrm{d}(\tau)$. Integral of the electric field is also defined as its vector potential A_d. Image adapted from [44]

acceleration $\mathbf{a}(t)$ to have a final drift velocity

$$\mathbf{v}_\mathrm{d}(t_\mathrm{f}, t_\mathrm{i}) = \mathbf{v}_0(t_\mathrm{i}) + \int_{\mathrm{t_i}}^{t_\mathrm{f}} \mathbf{a}(t)dt = \mathbf{v}_0(t_\mathrm{i}) - \int_{\mathrm{t_i}}^{t_\mathrm{f}} \mathbf{E}(t)dt.$$

In atomic units, $e = 1$ and $m_\mathrm{e} = 1$ so, they have been omitted from the equation. In photoconductive sampling, the drift of the electron is only measured along $\hat{\mathbf{E}}_\mathrm{drive}$. In the classical model, any newly ionized electron will have zero initial velocity in that direction as the injection field is orthogonal to the drive one— $\mathbf{v}_0(t_\mathrm{i})||\hat{\mathbf{E}}_\mathrm{drive} = 0$. If there were no scattering and no medium boundaries, the final velocity would remain unchanged till $t_\mathrm{f} \to \infty$.

$$\mathbf{v}_\mathrm{d}(t_\mathrm{f}, t_\mathrm{i})||\hat{\mathbf{E}}_\mathrm{drive} \coloneqq v_\mathrm{d}(t_\mathrm{i}) = -\int_{\mathrm{t_i}}^{t_\mathrm{f}\to\infty} \mathbf{E}_\mathrm{drive}(t')dt'.$$

The vector potential of an electromagnetic wave is

$$\mathbf{A}(t) \coloneqq \int_{\mathrm{t}}^{\infty} \mathbf{E}(t')dt',$$

so,

$$v_{\mathrm{d}}(t_{\mathrm{i}}) = -\mathbf{A}_{\mathrm{drive}}(t_{\mathrm{i}}).$$

The total drift current S_{d} measured at the end of the pulses is the time integral over the charged carrier creation rate times their final velocity:

$$S_{\mathrm{d}} = -\int_{-\infty}^{\infty} v_{\mathrm{d}}(t_{\mathrm{i}})\Gamma(\mathbf{E}_{\mathrm{inj}}, t_{\mathrm{i}})dt_{\mathrm{i}} = \int_{-\infty}^{\infty} \mathbf{A}_{\mathrm{drive}}(t_{\mathrm{i}})\Gamma(\mathbf{E}_{\mathrm{inj}}, t_{\mathrm{i}})dt_{\mathrm{i}}\,. \tag{4.1}$$

By delaying the injection pulse relative to the arrival of the drive field, the moment of ionization can be controlled. The number of electrons ionized at time t changes, changing the observed total drift current S_{d}. This simply shifts the moment of the ionization on the time axis with respect to the drive pulse. The drift current thus depends on the delay τ.

$$S_{\mathrm{d}}(\tau) = \int_{-\infty}^{\infty} \mathbf{A}_{\mathrm{drive}}(t)\Gamma(\mathbf{E}_{\mathrm{inj}}, t-\tau)dt \tag{4.2}$$

If the ionization is much shorter than an oscillation period of the drive field, it can be approximated with a delta function, in which case the measured signal is a replica of the drive pulse's vector potential:

$$S_{\mathrm{d}}(\tau) \approx \int_{-\infty}^{\infty} \mathbf{A}_{\mathrm{drive}}(t)\delta(t-\tau)dt = \mathbf{A}_{\mathrm{drive}}(\tau),$$

up to some multiplicative constant. The classical model is also the main motivation behind the specific form of Equation 4.3, which defines the same interaction much more generally.

4.3.2. General Description

Quantum mechanically, the drift current is related to the expectation value of an operator that requires the solution of a complicated time-dependent Schrödinger equation. The equation must simultaneously account for the binding potential of the medium and two optical fields. While the classical picture yields fruitful phenomenological simplification, the reality is quantum mechanical. In what follows I reconcile the classical and quantum mechanical models of photoconductive sampling. In photoconductive sampling one may assume that the injection field plays the role

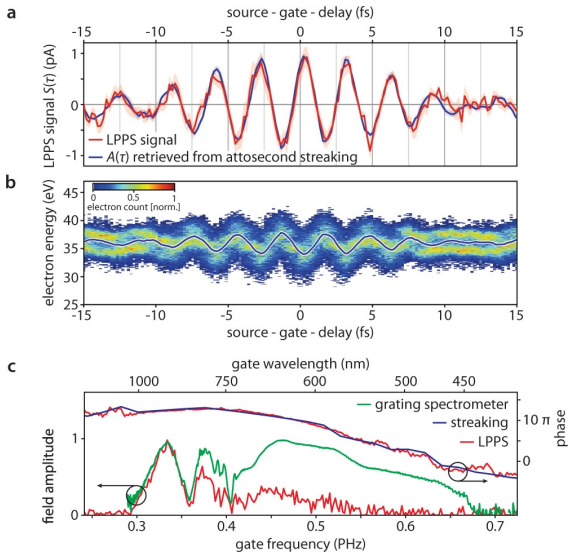

Figure 4.3.: A similar setup to one illustrated in Figure 4.2. This experiment is performed using linear photoconductive sampling (see chapter 4) in lithium fluoride. **a** is a normalized plot comparing the measured drift current (red) with the vector potential found using attosecond streaking (blue). The shaded region depicts the uncertainty. **b** shows spectrogram that is used to retrieve compare the data against a more mature technique— attosecond streaking(chapter 5). **c** compares the two results in the frequency domain. The plot in green is not relevant for this discussion. Taken from [45]

of inducing arbitrarily complicated charge carrier dynamics. Like the camera analogy earlier, if these dynamics last for a very short time, they can be used as a **gate** to sample another optical field that arrives with a delay τ. Thus, all injection pulse induced dynamics can be encapsulated by a **gating function** $G(t-\tau)$. The vector potential of the drive field is then gated by $G(t-\tau)$, such that only a small part of it can modify the charge carrier distribution whose effect is then felt at the electrodes. The electrodes work like a an integrating detector, giving the delay-dependent drift current:

$$\mathbf{S}_{\mathrm{d}}(\tau) = \int_{-\infty}^{\infty} \mathbf{A}_{\mathrm{drive}}(t) G(t-\tau) dt, \tag{4.3}$$

i.e., a convolution between the gating function and the vector potential of the drive field. For a general description, I could have also used a convolution of the drive electric field and the gating function. However, it will limit the extent to which I may draw parallels with the classical interpretation, while having no benefits.
This description only assumes one critical piece of information: **the gating function**,

however complicated, **remains unaffected by the drive field**. If the gating function creates a measurable drift current, it can be easily treated as a constant background. Within the domain of the assumption's validity, the general description works irrespective of the nature of the light matter interaction involved. The time duration during which the drive vector potential gets through the gate determines if the potential can be resolved in time. Reducing the duration that the gate 'opens' for and expanding the domain of vector potential over which the primary assumption remains valid, lies at the heart of improving the photoconductive sampling.
In frequency domain, the same equation simplifies to

$$S_{\mathrm{d}}(\omega) = A_{\mathrm{drive}}(\omega)G^{\star}(\omega) \tag{4.4}$$

and the domain where the general description is valid is quite easy to see. If

$$G(\omega) = \left(\frac{S_{\mathrm{d}}(\omega)}{A_{\mathrm{drive}}(\omega)}\right)^{\star}$$

is the same irrespective of A_{drive} , that is, it scales linearly with respect to drive field, the equations I presented are exact. The time resolution of the gating function is the inverse of the highest frequency at which $G(\omega)$ still has an amplitude strong enough to overcome the noise in the laboratory conditions.
If we limit the charge carrier generation to a duration of a few attoseconds, we can resolve a field with that finesse. How beautiful the results of the actual measurement are, i.e., how identical S_{d} is to A_{drive} is a matter of the exact functional form of $G(t)$. The more delta-like it is, the better.

4.3.3. The Gating Function Versus Ionization Rate

As I hinted in subsection 4.3.1, finding the ionization rate $\Gamma_{\mathrm{ion}}(t)$ is highly nontrivial. First, there are multiple definitions of instantaneous ionization probability in the presence of a strong external electric field, and all these general definitions contain an ad hoc component. Second, if one of such definitions works well for a particular experiment, it may fail at describing another time-resolved measurement of ionization dynamics.
Within the context of photoconductive sampling the **ionization rate** is the **classical interpretation** of the **gating function**. I never have to ask when an electron is ionized and can simply solve for the delay-dependent drift current. With a known drive field, the gating function and therefore the ionization rate is simply a deconvolution away. In fact, if I could obtain an analytical expression for the drift current, I might have a chance at obtaining the analytical form of the gating function itself!

I try finding this analytical form using SFA described in chapter 3. There is a caveat though. Although it is guaranteed that the classical model of photoconductive sampling will produce correct results as long as one uses the correct $G(t)$ as the ionization rate, the physics that $G(t)$ describes may not be limited to producing free charge carriers. In particular, complex nonlinear interactions between the injection and drive pulses may affect the motion of electrons, and the correct $G(t)$ will encode such processes. It is a matter of interpretation whether processes that the classical model does not explicitly account for should be regarded as a part of the ionization rate. I will do so in this thesis.

4.3.4. Linear Photoconductive Sampling

Linear photoconductive sampling (LPS), as the name suggests, achieves charge carrier injection in the medium via a linear interaction between the electrons bound in the medium and the injection pulse photons. The injection pulse is chosen such that the absorption of a single photon creates a charge carrier, just like in the conventional photoelectric effect [46]. Due to the linear relation, shorter pulses result in shorter injection durations. While it can have certain advantages over existing techniques like better signal to noise ratio [45], LPS still requires a vacuum chamber if the air can absorb the injection pulse.
When compared to the physics described in the next section, linear relations are easier to control and understand. Thus, linear photoconductive sampling serves as a valuable tool to benchmark an experimental setup and test if everything else works as expected. The best part is that with only a 'small' modification to this setup one may achieve the promised goal of ambient condition attosecond resolution. The next section will elaborate more on this.

4.3.5. Nonlinear Photoconductive Sampling

The change teased previously is quite simple— exploitation of nonlinearity for nonlinear photoconductive sampling (NPS). In the context of a laser pulse, a nonlinear process would be an interaction resulting from the simultaneous involvement of multiple photons. These photons are not always of the same frequencies/energies. Even when a single photon is not energetic enough to create a free charge carrier, the combined energy of N photons, such that $N \times E_{\text{photon}} > E_{\text{ion.}}$, can. This is a higher order process and can only occur with extremely high intensity field, i.e., by compensating the reduced cross-section with number of photons available. As elaborated in chapter 3, semi-classically, one describes this as the electric field being large enough to lower the Coulomb barrier, letting the electron tunnel out, with assistance from additional photons. Since the intensity of a linearly polarized light

changes in time, only those parts of the light pulse contribute to ionization that exceed a "cut-off" intensity.
If we use an injection pulse that is well controlled, easily characterized, and yet short enough that the part that can inject charge carriers lasts less than half a femtosecond, we may be capable of resolving fields in attoseconds in ambient conditions. In fact, this has already been successfully demonstrated [44]. Figure 4.4 illustrates the idea I explained so far. A successful measurement using this technique would result in

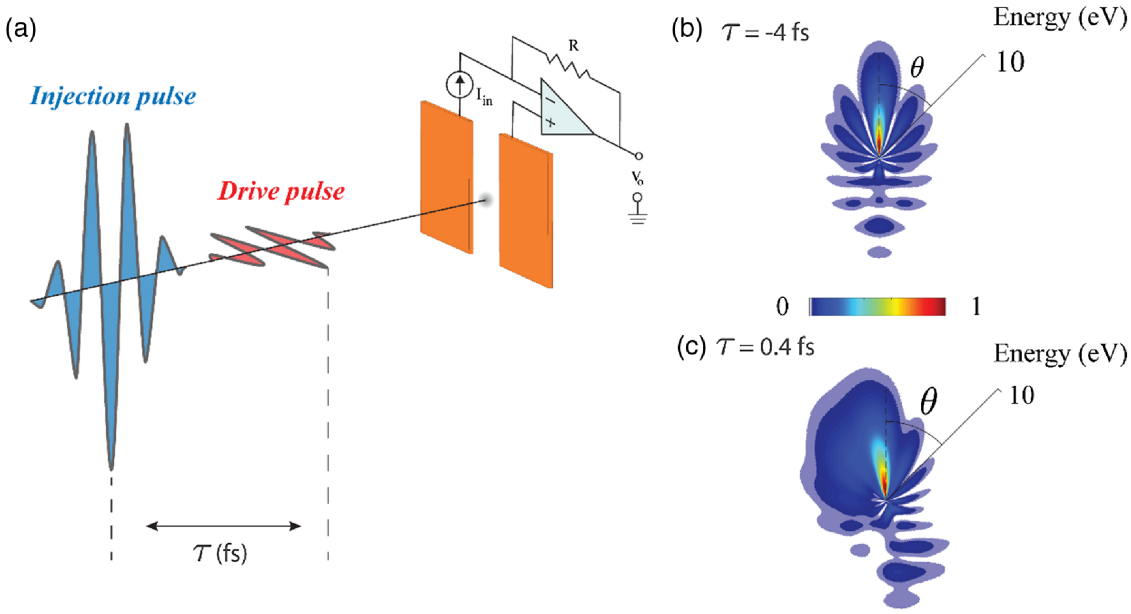

Figure 4.4.: A similar setup to one illustrated in Figure 4.2. This experiment is performed in a gas. Analogous to the previous experiment, **a** depicts the two orthogonal pulses. The injection pulse is strong enough to initiate nonlinear processes. **b** shows a time delay where the drive pulse does not overlap with the injection event. It results in a symmetric distribution of electrons. On the other hand, **c** shows a delay where the drive pulse arrives during the injection process and clearly skews the electron distribution to create an observable current [16]

traces like ones depicted in Figure 4.5

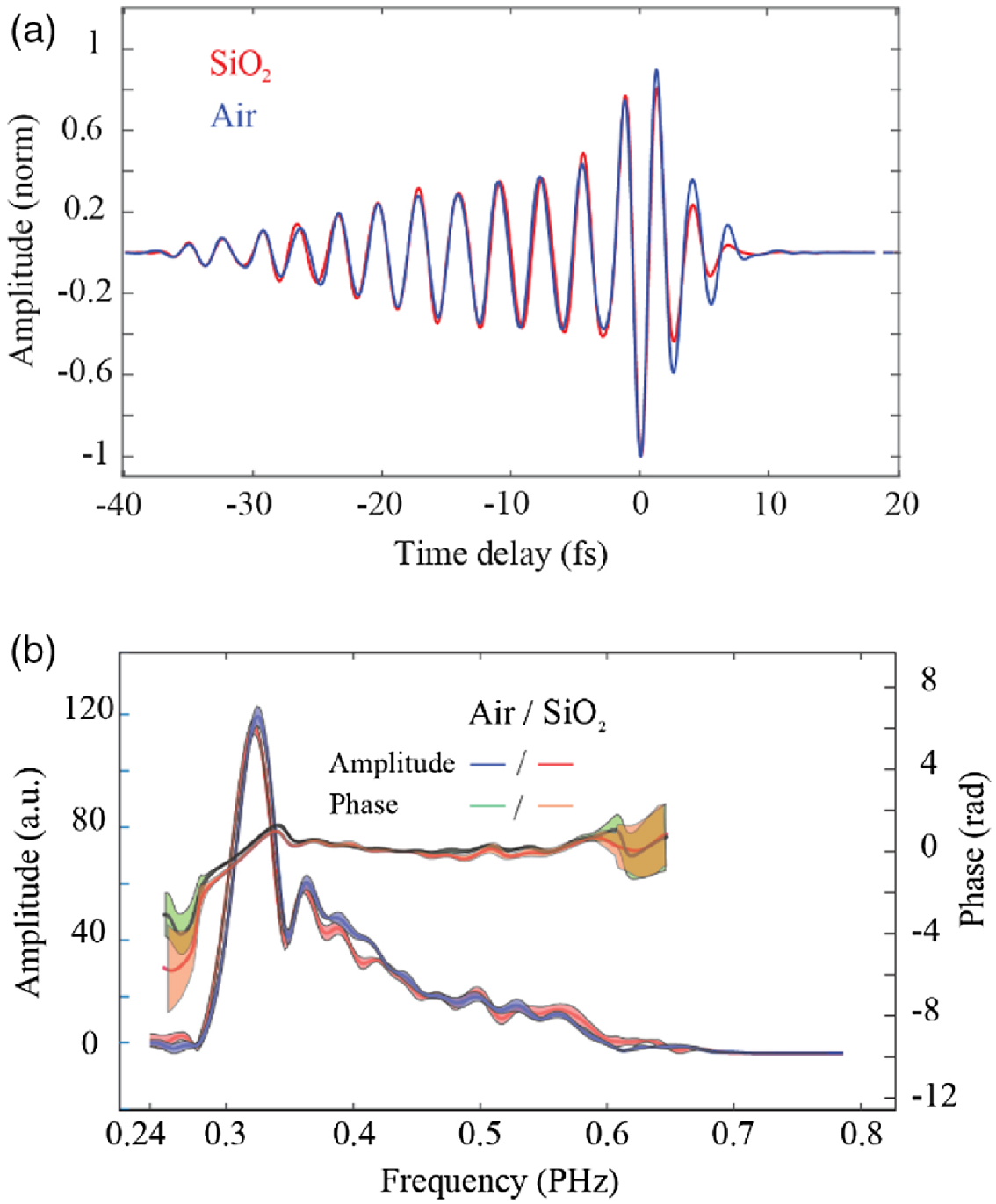

Figure 4.5.: **a** shows the normalized current obtained from an entire delay scan, for different mediums. As will be explained later, this shall have a one-to-one correspondence with the vector potential of drive field. In **b** we can inspect the same in the frequency domain [16]

5. Alternative techniques

The focus of this thesis is on photoconductive sampling. As I highlighted in chapter 4 the theoretical groundwork for photoconductive sampling results in the gating function. Even though it is a rigorous definition of ionization rate only within the context of photoconductive sampling, it is possible that the gating function is just as effective at predicting the ionization rate in other, similar experimental techniques. Here, I discuss two such techniques, but my theoretical results can be applicable for a much broader class of ideas that involve controlling charge carrier production rate.

5.1. Attosecond Streaking

Attosecond streaking predates photoconductive sampling. In fact, using this technique, sub-femtosecond time resolution of the optical field was achieved for the first time [47]. The breakthrough happened after it was realized that using a process called high harmonic generation [48], it is possible to generate light pulses with durations that are shorter than a femtosecond [40]. Using the previously mentioned analogy of a camera, once the shutter (short light pulse) was found, resolving optical fields that are slower than this shutter is simply a matter of defining a useful, measurable physical interaction between the two fields.
The experimental setup for attosecond streaking is like that of LPS in gases. It would look like Figure 4.4 with the strong injection pulse replaced by a weak attosecond pulse, the medium being a gas and the electrodes used to measure the current being replaced by photoelectron spectrometer that resolves the energy of the photoelectron reaching it, giving the attosecond streaking spectrogram. For a given delay between the two pulses, the setup measures the energy distribution of ionized electrons.
As proven in [8], measuring the photoelectron spectrum allows simultaneous determination of both the drive and the injection field. At time t_i, an attosecond pulse will generate photoelectrons with kinetic energy

$$E_\mathrm{kin} = \frac{m_\mathrm{e} v_0^2}{2} = \hbar\omega_\mathrm{i} - W_\mathrm{b}.$$

The time dependent drive field will modify the velocity of the free photoelectron, which calculated classically will be

$$\mathbf{v}(t) = -\frac{e}{m_\mathrm{e}}\mathbf{A}_\mathrm{drive}(t) + \left[\mathbf{v}_0 - \frac{e}{m_\mathrm{e}}\mathbf{A}_\mathrm{inj}(t-\tau)\right]$$

Two things determine the measured photoelectron spectrum:

1. The delay τ between the arrival of $A_\mathrm{drive}(t)$ and $E_\mathrm{inj}(t)$.
2. How broad $E_\mathrm{inj}(t)$ is in frequency domain (bandwidth) and whether the frequency of the injection signal is increasing or decreasing with time (up/down-chirp).

Both the injection and the drive pulse can be retrieved from the attosecond streaking spectrogram using a reconstruction algorithm [49, 50]. If the process is modeled as the transition between the ground state and the Volkov state (SFA) the delay dependent spectrogram $S(p,\tau)$ is given by

$$S(p,\tau) = \left|\int_{-\infty}^{\infty} dt \mathbf{E}_\mathrm{XUV}(t-\tau)\cdot\mathbf{d}(\mathbf{p}+\mathbf{A}(t))e^{itW_\mathrm{b}}e^{-i\int_\mathrm{t}^{\infty}dt'[\mathbf{p}+\mathbf{A}(t')]^2}\right|^2$$

Attosecond streaking spectrogram contains information about the momentum distribution of the free charge. This information is completely missing in photoconductive sampling as the drift current is the cumulative effect of this momentum distribution. The extra information allows attosecond streaking to resolve the injection field in addition to the drive. This might suggest that photoconductive sampling is a step backwards from streaking. However, the difference lies in need. Compared to the setup required for measuring the drift current, obtaining a spectrogram is harder. Unlike streaking, the injection pulse required for NPS has a longer duration. As the technology to generate short pulses matures, the requirement of resolving the injection pulse for every measurement can be supplanted by the reliability and reproducibility of pulse generation.

5.2. TIPTOE

The setup for Tunneling Ionization with a Perturbation for the Time-Domain Observation of an Electric Field (TIPTOE) is like that of NPS. The goal is still the time resolution of the electric field of the drive pulse- $E_\mathrm{drive}(t)$. Although the injection field E_inj is still used to create short bursts of photoelectrons, $E_\mathrm{drive}(t)$ no longer plays the role of an accelerating field. $E_\mathrm{drive}(t)$ is now polarized in the same

direction as E_{inj} and instead of accelerating electrons modifies the very process of photo-electron creation. The technique exploits the well-known notion of quasi-static tunneling ionization, which can be computed using Equation 3.1, to argue why such a setup allows resolving $E_{\text{drive}}(t)$. If E_{inj} photo-ionizes N_0 electrons, if E_{drive} is weak enough, its effects can be treated as the first order perturbation yielding $N_0 + \delta N$ electrons. Since the roles played by the two pulses are different from photoconductive sampling, in literature, injection pulse is usually referred as the fundamental pulse E_{F} and the drive pulse as the signal pulse E_{S}. Barring Figure 5.1 taken directly from a paper [10], I try maintaining the same nomenclature as photoconductive sampling to draw parallels with NPS.
By measuring both N_0 and $N_0 + \delta N$ simultaneously as shown in Figure 5.1 it is possible to reconstruct the drive field. Using the ADK equation of quasi-static

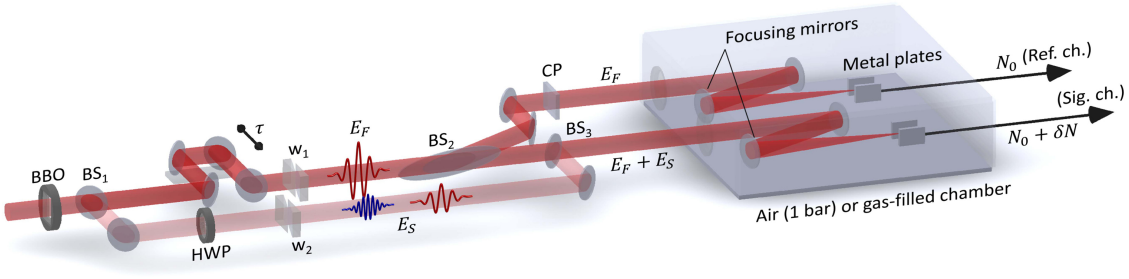

Figure 5.1.: Experimental setup of TIPTOE. In one arm, the injection field, E_{F} ionizes N_0 electrons. In the other one, the injection field and the drive field combined, $E_{\text{F}} + E_{\text{S}}$, excite $N_0 + \delta N$ electrons. The setup also shows how the mirrors are setup up for E_{F} to allow changing the distance between them, thereby changing the delay τ between the injection and the drive field. Image adapted from [10]

ionization rate for a given field strength, $W_{\text{ADK}}(E)$ (Equation 3.1), the ionization yield for a medium interacting solely with the injection pulse will simply be

$$N_0 = \int W_{\text{ADK}}(E_{\text{inj}})dt$$

once this interaction is additionally perturbed with the drive pulse using first order term of the Taylor expansion, one obtains

$$N_0 + \delta N = \int dt \left[W_{\text{ADK}}(E_{\text{inj}}(t)) + \left.\frac{dW_{\text{ADK}}(E)}{dE}\right|_{\text{E=E}_{\text{inj}}(\text{t})} \cdot E_{\text{drive}}(t) \right].$$

By changing the relative delay τ between the two pulses, the exact modification made to the unperturbed ionization rate changes, yielding different $\delta N(\tau)$. From this it is quite clear that

$$\delta N(\tau) \propto E_{\text{drive}}(\tau)$$

and measuring the net change in ionization yield allows to directly find $E_{\text{drive}}(t)$ up-to a multiplicative factor. Although I used the ADK formula to explain TIPTOE the concept remains valid so long as one remains within the quasi-static tunneling regime (ionization only depends on instantaneous total field intensity). Since the multiplicative factor is independent of the drive field, for a given injection pulse, it can be ascertained once with a known drive pulse, and then be used for resolving other unknown drive pulses.
Recently, it was shown that it is possible to remove the restriction of having a weak drive pulse by using a reconstruction algorithm [51]. It relies on higher order expansions with respect to the drive field and the known relation between the ionization rate and the electric field intensity in the multi-photon ionization regime (Equation 3.3).
TIPTOE is especially relevant to this thesis as it has the same goal as NPS: sub-femtosecond optical field resolution without using an attosecond pulse. At a fundamental level TIPTOE differs from NPS by requiring a perturbative expansion in its very premise. By looking at the first and the second derivatives of the ADK quasi-static ionization-rate a practical difference between NPS and TIPTOE is also brought to light. The increase in signal with respect to increasing injection field strengths will be more prominent in NPS, allowing NPS to resolve weaker fields. Additionally in the form I presented, TIPTOE cannot be extended beyond the quasi-static regime as the proposed expansion only works when ionization reacts instantly to the change in field strength. Analysis presented in part III of this thesis suggests that the shortest possible injection burst that can be generated by a pulse exists for field strengths where quasi-static models do not apply. Thus, any technique limited to quasi-static tunneling cannot exploit nonlinear electron injection to its full potential.

6. Ab Initio Simulations

SFA is an analytical theory. However, it makes several assumptions about the process of ionization which, depending on the electromagnetic field and the medium, can be very wrong. For any results obtained from the SFA, it is useful to check it against ab initio simulations. Ab means "from" and initio means "beginning". The name refers to the fact that these simulations try to compute physical observables with the most basic information about the experimental setup. For photoconductive sampling, an ab initio simulation would ideally be able to predict the delay-dependent drift current with the information about the laser pulses and the optical medium used. There can be a difference in the order of magnitude between the SFA and the ab initio results, as I will highlight in chapter 10, but there should be a qualitative agreement. If both agree, one may rejoice in the fact that the SFA suffices to capture everything of interest. If there is a discrepancy, finding the exact physical process responsible for this is useful by itself.
My thesis concentrates on electromagnetic waves impinging on a hydrogen atom. So, I need to solve the time-dependent Schrödinger equation for a single electron in the presence of a constant Coulombic potential and an electromagnetic field that changes with time.
As was explained in chapter 4, the delay-dependent drift current is the result of the interaction of the medium with two orthogonally polarized laser pulses. If the delay between the two pulses is changed, the net field experienced by the medium, here, the hydrogen atom, is fundamentally different. To reflect this physical reality, every delay point needs to be set up as an independent simulation. For a delay scan sampled at seventy points, seventy similar but individual simulations are needed. Thus, numerical simulations of photoconductive sampling are very time consuming and resource intensive.
Implementing a numerical solver for the time dependent Schrödinger equation is a complex task. Fortunately, there are groups dedicated to developing open-source packages allowing simulations for a broad range of problems. There are no exact solutions for most time-dependent Schrödinger equation problems, so each package approaches the numerical problem differently with distinct sets of assumptions, each with its own pros and cons. A researcher needs to choose a package that is most appropriate for the physical problem at hand. As I am interested in hydrogen atoms, for reasons that I will elaborate upon in the following sections, I chose a package

called tRecX [52].

6.1. Time-Dependent Recursive Indexing

Based on what external conditions and potentials it is being subjected to, simulations of the hydrogen atom can be very cumbersome. There is no screening, and the Coulomb potential extends all the way to infinity. Most packages need an extremely large simulation volume to capture this. A larger volume corresponds to more discrete grid points making each simulation much more time and memory intensive. tRecX, Time-dependent Recursive indeXing, employs a combination of the surface flux method and exterior complex scaling to circumvent these problems. A typical simulation with the hydrogen atom takes a few minutes rather than hours. Quoting directly from the abstract of the tRecX documentation, "tRecX is a C++ code for solving generalized inhomogeneous time-dependent Schrödinger-type equations $id\Psi/dt = H[t, \Psi] + \phi$ in arbitrary dimensions and in a variety of coordinate systems. The operator $H[t, \Psi]$ may have simple nonlinearity, as in Gross-Pitaevskii and Hartree(-Fock) problems. Primary application of tRecX has been non-perturbative strong-field single and double photo-electron emission in atomic and molecular physics." [52]
The package uses two theoretical innovations. Having a brief overview of these ideas is useful as it may help prevent the pitfall of interpreting a numerical artifact as a physical one.

6.1.1. irECS—Infinite Range Exterior Complex Scaling

I am only summarizing the main idea of complex scaling. For more information, the reader is referred to [53].
For hydrogen atom in the presence of an electromagnetic field, a numerical solution to the TDSE is hard as the Coulomb potential decays as $1/r$. I need it to disappear much faster, ideally exponentially fast. Without that, the boundary of the simulation box, if not large enough, will have numerical issues with all the wave packets reaching it. There will be nonphysical reflected incoming packets created by the discontinuity at the boundary.
For sane computational resource requirements, I want things to converge in a short space rather than having to reach infinitely large distances. To solve this conundrum, one could try scaling the real space: $z_\lambda(x) = e^\lambda x$, and artificially make the simulation box smaller. This is a unitary transformation, so the physics remains the same, albeit 'scaled'. One could take this a step further and do an exterior scaling, that is,

coordinates get scaled only outside a certain boundary:

$$\mathbf{x} \to z_{\lambda \mathrm{R}_0}(\mathbf{x}) = \begin{cases} \mathbf{x} & \text{for } x < R_0, \\ e^{\lambda}(\mathbf{x} - R_0) + R_0 & \text{for } x > R_0. \end{cases} \tag{6.1}$$

While distances do get scaled, my numerical problem remains just as challenging. The simulation size is smaller, but the points needed to resolve everything will need to be closer, resulting in a similar grid density. The transformation

$$H_{\lambda \mathrm{R}_0} \Psi_{\lambda \mathrm{R}_0} = U_{\lambda \mathrm{R}_0} H U^*_{\lambda \mathrm{R}_0} \Psi_{\lambda \mathrm{R}_0} = U_{\lambda \mathrm{R}_0} H \Psi,$$

with

$$U_{\lambda \mathrm{R}_0} \Psi(\mathbf{x}) = \begin{cases} \Psi(\mathbf{x}) & \text{for } x < R_0 \\ e^{\lambda/2} \Psi(e^{\lambda}(\mathbf{x} - R_0) + R_0) & \text{for } x > R_0 \end{cases}$$

does not achieve much.
As a second attempt, I do not try to change the magnitude of the distances but make the large assumption that an analytical continuation is possible and simply rotate things in the complex plane, $\lambda \to i\Theta$ –an exterior complex scaling (ECS). The continuum spectra are now rotated by an angle of 2Θ into the lower complex plane. Turns out, this has a major advantage for the wave function. At the boundary, outgoing waves can be easily distinguished from the incoming ones as only the outgoing ones may be normalized. As a demonstration, for a plane wave with momentum p:

$$e^{+ipx} \to e^{+ipR_0} e^{+ip\cos\theta(x-R_0)} e^{-p\sin\theta(x-R_0)} \tag{6.2}$$

A wave with a positive p (outgoing) dies out exponentially with x while the incoming one ($p \to -p$) explodes. By limiting the solution space to square integrable functions all nonphysical incoming reflections are automatically removed. I can now get away with much smaller simulation boxes. For ECS, an analytical continuation is possible if the potentials involved are 'dilation analytic' but that is hard to prove. Instead, one can numerically confirm that the modified Hamiltonian produces the same dynamics as the unmodified one and that for all $|x| < R_0$, the solution is identical to that of the original.
The part of ECS requiring special finesse is the treatment of the discontinuity at R_0, which can have its own set of reflections. If the scaling is smooth, the discontinuity will not result in any nonphysical reflections. This is where the infinite range part of irECS comes into play. In irECS, the complex scaled region extends all the way to infinity, which seems to resolve any R_0 discontinuity related problem, and turns an inaccurate ECS [54] into a perfect absorber, that is, no nonphysical reflections. This is confirmed numerically up to machine precision [53]. Furthermore, it allows extracting information of dynamics beyond the unscaled region— a fact that is especially useful for calculating the drift current described in detail in chapter 7.

6.1.2. tSurff and iSurff—Time-Dependent and Infinite Time Surface Flux Methods

When talking about drift current, I often mentioned the free charge carriers. What do I even mean by that? Limiting the context to the binding potential of an atom, it refers to an electron being in a continuum state. For a given physical system the continuum is the region of space beyond the binding influence of the potential, so, an electron in the continuum can propagate to infinity with a gentle push. To calculate the drift current information about the continuum states at any given moment in time is necessary. However, the continuum is infinitely large and storing information about wavefunction that exist in an infinitely large space can be troublesome.
The time dependent surface flux method [55] is based on the simple idea of calculating the time integral of the flux leaving a surface $|\mathbf{x}| = R_0$ instead of the entire wave function. Only the wave function inside the volume defined by the surface is computed. This is a lot more efficient than first calculating and then projecting the entire wave-function onto continuum states. If the absorption defined beyond this surface by complex scaling truly does not create nonphysical reflections, the two methods are analytically equivalent [55]. If the hypothesis of irECS mentioned in previous section is true, and it indeed is a perfect absorber, tSurff should provide exact results.
The dynamics inside an atom do not stop long after the laser pulses are gone. Certain electrons can be freed but have slow wave-packets that take forever to reach the surface $|\mathbf{x}| = R_0$ to be observable. This would be problematic when measuring quantities related to the presence of free electrons. For quantities like ionization probability or as in my case, the drift current, we want results at $t \to \infty$. In the time dependent version of the surface flux methods, one simply waits till all the wave-packet inside the un-scaled region has left the surface, that is, things have stopped changing. It works but requires extra computational time and is still not mathematically exact. One can avoid waiting if the eigenfunctions of the laser-field-free Hamiltonian (here hydrogen) are known analytically. Instead of waiting, we can project the wavefunction inside the volume obtained at the end of all the laser pulses on these eigenfunctions. Since there are no other perturbations, these are exact, and we can analytically evolve them in time. This would directly yield the infinite time results without any ambiguity. A formal proof can be found in [56]. I am not providing it here as it is straightforward and does exactly what I described.

Part II.

Analytical Theory

7. Delay-Dependent Residual Drift Current

As already described in chapter 4, photoconductive sampling requires two orthogonally polarized laser pulses impinging on a medium to create a measurable electric current. The first pulse, the drive one, has an unknown field we would like to resolve. The goal is to quantify this field by using a short burst of free charge carriers created by a second, known injection pulse. Mathematically, the short burst of charge carriers is equivalent to a gating signal that can take a small "snippet" of the drive field in time. There are multiple ways to formulate this measurement but Equation 4.3:

$$S_{\mathrm{d}}(\tau) = \int_{-\infty}^{\infty} A_{\mathrm{d}}(t) G(t-\tau) dt,$$

is particularly convenient. As shown in chapter 4, it has a direct connection to the classical interpretation. To measure the drive field using this technique, the gating function $G(t)$ must be fully determined by injection pulse, the only assumption required for Equation 4.3 to remain true. With this the vector potential of the drive pulse can be sampled. For example, if $G(t)$ were a delta function, the drift current would be exactly equal to the vector potential of the drive pulse. With precise control over the injection process one can shape the gating function to get increasingly precise traces of the drive field.

7.1. Derivation under the Strong Field Approximation

I use Equation 3.8 for the SFA continuum state as the starting point for calculating the current,

$$\begin{aligned} |\Psi(\mathbf{p})\rangle = -i\,|\mathbf{p}\rangle \int_0^{\infty} dt' e^{-\frac{i}{2}\int_{t'}^{\infty}[\mathbf{p}+\mathbf{A}(t'')]^2 dt''} e^{+iW_{\mathrm{b}}t'} \\ \langle \mathbf{p}+\mathbf{A}(t')|\,\mathbf{d}\cdot\mathbf{E}(t')\,|\phi_0\rangle \end{aligned} \tag{7.1}$$

The drift current is an experimental observable. It can be mapped to the expectation value of the projection of the momentum of the free electron along the direction of

measurement. The end-goal of all the analysis that follows is to reform the equation obtained for the drift current into something like Equation 4.3, while making as few approximations as possible. The equation can then be implemented to find the drift current. The specific form of the equation would further yield an analytical formula for the gating function as I will show in chapter 8. This would be especially useful as I could then avoid having to set up individual simulations for every delay point. With the gating function, the drift current is just one time convolution away.
The direction of the current measured at the electrodes is such that it corresponds to the velocity of the electron projected in the direction parallel to the polarization of the drive field. Without loss of generality, I assume that the drive field is polarized along the x-axis and the injection field is polarized along z. Then,

$$\langle S_\mathrm{d} \rangle \propto \int d\mathbf{p} \int d\mathbf{p}' \, \langle \Psi(\mathbf{p}')| - \hat{p}_x \, |\Psi(\mathbf{p})\rangle \tag{7.2}$$

The delay τ is absent from this and all subsequent equations as it just amounts to replacing the injection field with a version shifted along the time axis.
Since the ground state remains unaffected until the optical field arrives at $t = 0$, I am setting the lower limit of the integral to $t \to -\infty$.

$$\begin{aligned} \langle \hat{p}_x \rangle = \int d\mathbf{p} d\mathbf{p}' \int_{-\infty}^{\infty} dt_1 \int_{-\infty}^{\infty} dt_2 \, \langle i\mathbf{p}' | \, p_x \, | -i\mathbf{p} \rangle \\ \times \exp\left(i I_\mathrm{p} (t_2 - t_1) + \frac{i}{2} \int_{t_1}^{t_2} dt'' [\mathbf{p} + \mathbf{A}(t'')]^2 \right) \\ \times \langle \phi_0 | \, \mathbf{E}^\star(t_1) \cdot \mathbf{d}^\star \, | \mathbf{p} + \mathbf{A}(t_1) \rangle \, \langle \mathbf{p} + \mathbf{A}(t_2) | \, \mathbf{d} \cdot \mathbf{E}(t_2) \, | \phi_0 \rangle \end{aligned} \tag{7.3}$$

The integral over $\mathbf{p}'$ yields a delta function. The equation can be written more compactly:

$$\begin{aligned} \langle \hat{p}_x \rangle = \int d^3p \int_{-\infty}^{\infty} dt_1 \int_{-\infty}^{\infty} dt_2 p_x \exp\left(i I_\mathrm{p} (t_2 - t_1) + \frac{i}{2} \int_{t_1}^{t_2} dt'' [\mathbf{p} + \mathbf{A}(t'')]^2 \right) \\ \times (\mathbf{E}^\star(t_1) \cdot \mathbf{d}^\star[\mathbf{p} + \mathbf{A}(t_1)]) \, (\mathbf{d} \; [\mathbf{p} + \mathbf{A}(t_2)] \cdot \mathbf{E}(t_2)) \end{aligned} \tag{7.4}$$

Changing variables, $t = \frac{t_2 + t_1}{2}, T = \frac{t_2 - t_1}{2}$, gives:

$$\begin{aligned} \langle \hat{p}_x \rangle = 2 \int d^3p \int_{-\infty}^{\infty} dt \int_{-\infty}^{\infty} dT \, p_x \, \exp\left(2 i I_\mathrm{p} T + \frac{i}{2} \int_{t-T}^{t+T} dt'' [\mathbf{p} + \mathbf{A}(t'')]^2 \right) \\ \times (\mathbf{E}^\star(t - T) \cdot \mathbf{d}^\star[\mathbf{p} + \mathbf{A}(t - T)]) \\ \times (\mathbf{E}(t + T) \cdot \mathbf{d}[\mathbf{p} + \mathbf{A}(t + T)]) \end{aligned} \tag{7.5}$$

So far everything has been very general. In photoconductive sampling, $\mathbf{E}(t) = E_z(t)\,\mathbf{e}_\mathrm{z} + E_x(t)\,\mathbf{e}_\mathrm{x}$ and $\mathbf{A}(t) = A_z(t)\,\mathbf{e}_\mathrm{z} + A_x(t)\,\mathbf{e}_\mathrm{x}$. The directions z and x represent

the polarization directions of the injection and drive fields. Since I assume that the drive pulse cannot photoionize on its own, I can approximate the interaction potential with $V_{\mathrm{L}}(t) = \mathbf{E}(t) \cdot \mathbf{d} = (E_z(t)\,\mathbf{e}_{\mathrm{z}} + E_x(t)\,\mathbf{e}_{\mathrm{x}}) \cdot \mathbf{d} \approx E_z(t) d_z$.
Evaluating the integral over $\mathbf{p}$, any constant value can be added to it without changing the result. Let us apply the following substitution:

$$\mathbf{p} \mapsto \mathbf{p} + \mathbf{A}(t),$$

and then change to spherical coordinates for $\mathbf{p}$. I obtain:

$$\begin{aligned}\langle \hat{p}_x \rangle = 2 \int_{-\infty}^{\infty} dt \int_{-\infty}^{\infty} dT \int p^2 dp \sin\theta d\theta d\phi \, (p \sin\theta \cos\phi - A_x(t)) \\ \times \exp\left(2iI_{\mathrm{p}}T + \frac{i}{2} \int_{-\mathrm{T}}^{T} dt'' [\mathbf{p} + \mathbf{A}(t+t'') - \mathbf{A}(t)]^2 \right) \\ \times E_z^\star(t-T) E_z(t+T) \\ \times d_z^\star[\mathbf{p} + \mathbf{A}(t-T) - \mathbf{A}(t)] d_z[\mathbf{p} + \mathbf{A}(t+T) - \mathbf{A}(t)]\end{aligned} \tag{7.6}$$

Defining $\Delta(x) = \mathbf{A}(t+x) - \mathbf{A}(t)$:

$$\begin{aligned}\langle \hat{p}_x \rangle = 2 \int_{-\infty}^{\infty} dt \int_{-\infty}^{\infty} dT \int p^2 dp \sin\theta d\theta d\phi \, (p \sin\theta \cos\phi - A_x(t)) \\ \times \exp\left(2iI_{\mathrm{p}}T + \frac{i}{2} \int_{-\mathrm{T}}^{T} dt'' [\mathbf{p} + \Delta(t'')]^2 \right) \\ \times E_z^\star(t-T) E_z(t+T) \\ \times d_z^\star[\mathbf{p} + \Delta(-T)] d_z[\mathbf{p} + \Delta(T)]\end{aligned} \tag{7.7}$$

This is still not enough. Direct numerical integration of a highly oscillating function over four coordinates can be very time consuming and unstable. Moreover, it does not remotely reflect the ansatz in Equation 4.3. The second term inside the exponential function can be further simplified.

$$\begin{aligned}\frac{i}{2} \int_{-\mathrm{T}}^{T} dt'' [\mathbf{p} + \Delta(t'')]^2 &= \frac{i}{2} \int_{-\mathrm{T}}^{T} dt'' \left(p^2 + \Delta_z^2(t'') + \Delta_x^2(t'') + 2\mathbf{p} \cdot \Delta(t'') \right) \\ &= ip^2 T + \frac{i}{2} \int_{-\mathrm{T}}^{T} dt'' \left[\Delta_z^2(t'') + \Delta_x^2(t'') \right] \\ &+ ip\cos\theta \int_{-\mathrm{T}}^{T} dt'' \Delta_z(t'') + ip\sin\theta\cos\phi \int_{-\mathrm{T}}^{T} dt'' \Delta_x(t'')\end{aligned} \tag{7.8}$$

For convenience and compactness, I am defining

$$\overline{\Delta_{\mathrm{i}}^l} = \int_{-\mathrm{T}}^{T} dt' \Delta_{\mathrm{i}}^l(t') = \int_{-\mathrm{T}}^{T} dt' [A_{\mathrm{i}}(t+t') - A_{\mathrm{i}}(t)]^l. \tag{7.9}$$

It is at this point that an extremely useful expansion can be used to move some terms out of the exponential function! The Jacobi-Anger expansion [57] dictates

$$\exp\left(ip\sin\theta\cos\phi\overline{\Delta_x}\right) = J_0\left(ip\sin\theta\overline{\Delta_x}\right) + 2\sum_{\mathrm{n}=1}^{\infty} i^n J_{\mathrm{n}}\left(ip\sin\theta\overline{\Delta_x}\right)\cos(n\phi), \quad (7.10)$$

where J_{i} is the i^{th} Bessel function. With this, Equation 7.7 takes the following form:

$$\begin{aligned}\langle\hat{p}_x\rangle = 2\int_{-\infty}^{\infty}dt\int_{-\infty}^{\infty}dT\int p^2dp\int\sin\theta d\theta\int_0^{2\pi}d\phi\,(p\sin\theta\cos\phi - A_x(t))\\ \times\exp\left(2iI_{\mathrm{p}}T + ip^2T + \frac{\overline{\Delta_x^2}+\overline{\Delta_z^2}}{2} + ip\cos\theta\overline{\Delta_z}\right)\\ \times\left(J_0\left(ip\sin\theta\overline{\Delta_x}\right) + 2\sum_{\mathrm{n}=1}^{\infty} i^n J_{\mathrm{n}}\left(ip\sin\theta\overline{\Delta_x}\right)\cos(n\phi)\right)\\ \times E_z^\star(t-T)E_z(t+T)\\ \times d_z^\star[\mathbf{p}+\Delta(-T)]d_z[\mathbf{p}+\Delta(T)].\end{aligned} \quad (7.11)$$

So far, I have only managed to make complicated expressions worse. However, Equation 7.11 can be integrated over ϕ analytically! It yields the following result:

$$\begin{aligned}\langle\hat{p}_x\rangle = 2\int_{-\infty}^{\infty}dt\int_{-\infty}^{\infty}dT\int p^2dp\int\sin\theta d\theta\,(E_z^\star(t-T)E_z(t+T))\\ \times\left(-2\pi A_x(t)J_0\left(ip\sin\theta\overline{\Delta_x}\right) + 2\pi ip\sin\theta J_1\left(ip\sin\theta\overline{\Delta_x}\right)\right)\\ \times\exp\left(2iI_{\mathrm{p}}T + ip^2T + \frac{\overline{\Delta_x^2}+\overline{\Delta_z^2}}{2} + ip\cos\theta\overline{\Delta_z}\right)\\ \times d_z^\star[\mathbf{p}+\Delta(-T)]d_z[\mathbf{p}+\Delta(T)].\end{aligned} \quad (7.12)$$

Equation 7.12 is quite general. It contains certain assumptions and approximations that are implicit to SFA and others that I made during the illustrated derivation. I will summarize those altogether in chapter 10 when I consider the theoretical differences between my SFA results and ab initio results from tRecX.

7.2. Obtaining the Current from Ab Initio Results

For reproducibility of the results that I will present in Part III, I am providing the basic information of the input files used with tRecX (chapter 6). All tunable parameters that remain unchanged for a set of simulations are determined after careful convergence testing.

```
Title: Photoconductive Sampling -

Operator: hamiltonian='1/2<<Laplacian>>-<1><1><trunc[50,60]/Q>'
Operator: interaction='iLaserAz[t]<<D/DZ>>+iLaserAx[t]<<D/DX>>'

Spectrum: radialPoints=100, plot=total
Spectrum: expectationValues='<1><1><GridWeight>,
                              <1><Q><GridWeight*Q>,        # p_y
                            <cos(Q)><sqrt(1-Q*Q)><GridWeight*Q>,
                            <sin(Q)><sqrt(1-Q*Q)><GridWeight*Q>'
                              # <den(e) continuum, p_z, p_x, p_y>
ISurff: use=true

Axis: name,nCoefficients, lower end, upper end, functions, order
      Phi, 5
      Eta, 11, -1, 1, assocLegendre{Phi}
       Rn, BOX/4*ORD, 0, 60, polynomial, ORD
       Rn, 30, 60, Infty, polExp[0.5]

Absorption: kind, axis, theta, upper
                         ECS, Rn, 0.3, 60

Laser: shape, I(W/cm2), FWHM,lambda(nm),polarAngle, phiCEO, peak
    cos8, 1.0e+14, 1.00 OptCyc, 750, 00, 0, 0 s    # injection pulse
   cos8, 1.0e+9, 0.5e-15 s, 750, pi/2, 0, <drive pulse delay> s
      #drive

TimePropagation: end, print, store, cutEnergy, accuracy,fixStep
                      3.0 OptCyc,0.5 OptCyc, 1 au, 100, 1e-07,
                         0.025
```

The most important parts to pay attention to are the definition of the Hamiltonian, the two laser pulses and expectation values computed.
The Hamiltonian defines a hydrogen atom with a small modification—the Coulombic potential is exponentially suppressed beyond fifty atomic units and becomes zero at 60 atomic units. This is an approximation, and it was validated by ensuring that the numerical results remain unchanged even if these boundaries are shifted considerably.
The units have already been described in chapter 2. The polar angle defines the

polarization direction of the pulses. For a delay scan everything remains unchanged, except the peak of the second pulse. It defines when the peak intensity of the pulse arrives in time and can be changed to simulate different delays. The time grid used for the scan is determined based on Nyquist's Sampling Condition.
The last thing to pay attention to is the line, 'Spectrum: expectationValues'. This is the part of the package that allows calculation of expectation values in the continuum. For the drift current I am interested in calculating p_{x}. I additionally calculated the continuum electron density, p_{z} and p_{y} for testing purposes.

8. Gating Function

In the previous chapter, I had elucidated that Equation 7.12 can be further simplified to obtain the form promised in Equation 4.3. To remind the reader again, my final aim is to reformulate

$$\begin{aligned}\langle -\hat{p}_x(\tau)\rangle = -2\int_{-\infty}^{\infty} dt \int_{-\infty}^{\infty} dT \int p^2 dp \int \sin\theta d\theta \\ \times \exp\left(2iI_{\mathrm{p}}T + ip^2T + \frac{\overline{\Delta_x^2} + \overline{\Delta_z^2}}{2} + ip\cos\theta\overline{\Delta_z}\right) \\ \times \left(-2\pi A_x(t) J_0\left(ip\sin\theta\overline{\Delta_x}\right) + 2\pi ip\sin\theta J_1\left(ip\sin\theta\overline{\Delta_x}\right)\right) \\ \times E_z^\star(t-T)E_z(t+T) \\ \times \mathbf{d}_z^\star[\mathbf{p}+\Delta(-T)]\mathbf{d}_z[\mathbf{p}+\Delta(T)],\end{aligned}$$

into something that it looks like

$$S_{\mathrm{d}}(\tau) = \int_{-\infty}^{\infty} A_{\mathrm{d}}(t) G(t-\tau) dt.$$

If possible, I would have an analytical expression of the gating function. It will be useful to avoid having to simulate every single delay for a delay scan. Even more importantly, I can plot the exact gating function rather than indirectly obtaining it by a deconvolution based on Equation 4.3. In chapter 4, subsection 4.3.3, I argued that the gating function is indeed the ionization rate in the context of photoconductive sampling. An analytical form of the gating function directly yields information about the process of photoionization itself. With known drive pulses, one can experimentally confirm that the linear relation between the drive pulse and the drift current (Equation 4.3) is true, and one may reconstruct the gating function from these experimental results.
The only approximation needed to reformulate Equation 7.12 is expanding the Bessel function and dropping the higher order terms. Taking only the zeroth order

term of the expansion into account,

$$\begin{aligned}\langle \hat{p}_x(\tau)\rangle = 2\int_{-\infty}^{\infty} dt \int_{-\infty}^{\infty} dT \int p^2 dp \int \sin\theta d\theta \\ \times \exp\left(2iI_{\mathrm{p}}T + ip^2T + \frac{\overline{\Delta_x^2}+\overline{\Delta_z^2}}{2} + ip\cos\theta\overline{\Delta_z}\right) \\ \times \left(-A_x(t) + p\sin\theta\left(\frac{ip\sin\theta\overline{\Delta_x}}{2}\right)\right) \\ \times E_z^\star(t-T)E_z(t+T) \\ \times \mathbf{d}_z^\star[\mathbf{p}+\Delta(-T)]\mathbf{d}_z[\mathbf{p}+\Delta(T)],\end{aligned}$$

$$\begin{aligned}\implies \langle \hat{p}_x(\tau)\rangle = 4\pi\int_{-\infty}^{\infty} dt \int_{-\infty}^{\infty} dT \int p^2 \sin\theta d\theta \\ \times \exp\left(2iI_{\mathrm{p}}T + ip^2T + \frac{\overline{\Delta_x^2}+\overline{\Delta_z^2}}{2} + ip\cos\theta\overline{\Delta_z}\right) \\ \times \left(\underbrace{\frac{-A_x(t)(1+iTp^2sin^2\theta)}{}}_{:=\text{part 1}} + \underbrace{\frac{ip^2sin^2\theta}{2}\left[\int_{-\mathrm{T}}^{T} dt' A_x(t+t')\right]}_{:=\text{part 2}}\right) \\ \times E_z^\star(t-T)E_z(t+T) \\ \times \mathbf{d}_z^\star[\mathbf{p}+\Delta(-T)]\mathbf{d}_z[\mathbf{p}+\Delta(T)],\end{aligned} \tag{8.1}$$

Obtaining gating function is now only a matter of shuffling a few terms around. It can be checked numerically that the drift current obtained from this approximation is virtually indistinguishable from the original expression. Figure 8.1 supports this claim. The plot in red is the result of calculating the drift current without making any approximations or expansions. The Bessel functions are computed using python's SciPy library [58]. The plot in green calculates the delay dependent drift current by first computing the gating function, which requires approximations. The computed points of the two curves almost coincide. By comparing the sub-figures, I conclude that the minor deviations would converge with a higher density of the integral grid, but that was not possible due to limited RAM. The plot in gray is the vector potential of the drive pulse normalized to match the maxima of the other two. The overlap between the delay-dependent drift current and the vector potential is not exceptionally good as the injection pulse chosen in this example is incapable of creating a gating function to sample the drive field exactly. I chose this example to highlight the importance of choosing the injection pulse to tune the gating function

itself.

As already hinted in Equation 8.1, the expression is split in two parts such that

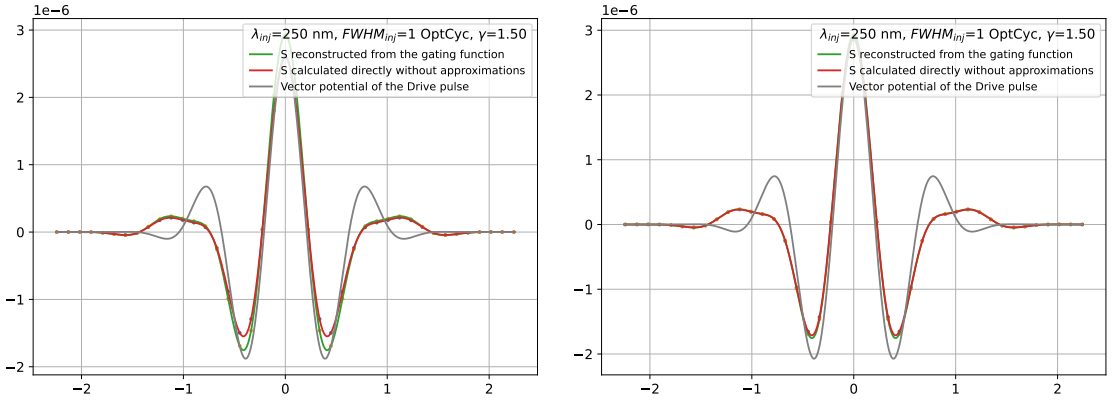

(a) Integral using coarse discretisation (b) Denser Integral grid

Figure 8.1.: Comparison of Delay-Dependent drift current obtained analytically with a version that makes approximations that are necessary to reformulate the equation to look like Equation 4.3

the part with an additional integral over the vector potential of the drive pulse can be handled separately.

$$\begin{aligned}\langle -\hat{p}_x(\tau)\rangle &= \langle S_1(\tau) + S_2(\tau)\rangle \\ &= \int_{-\infty}^{\infty} dt A_x(t)\, G(t-\tau) \\ &= \int_{-\infty}^{\infty} dt A_x(t)\, [G_1(t-\tau) + G_2(t-\tau)]\end{aligned}$$

$$\begin{aligned}\langle S_1(\tau)\rangle = \int_{-\infty}^{\infty} dt A_x(t) \cdot \int_{-\infty}^{\infty} dT \int 4\pi p^2 dp \sin\theta d\theta \\ \times \exp\left(2iI_\mathrm{p}T + ip^2T + \frac{\overline{\Delta_x^2} + \overline{\Delta_z^2}}{2} + ip\cos\theta\overline{\Delta_z}\right) \\ \times \left(1 + iTp^2\sin^2\theta\right) \\ \times E_z^\star(t-T)E_z(t+T) \\ \times \mathbf{d}_z^\star[\mathbf{p} + \Delta(-T)]\mathbf{d}_z[\mathbf{p} + \Delta(T)] \\ = \int_{-\infty}^{\infty} dt A_x(t)\, G_1(t-\tau) \quad .\end{aligned} \tag{8.2}$$

$$\begin{aligned}\langle S_2(\tau)\rangle = -\int_{-\infty}^{\infty} dt \int_{-\infty}^{\infty} dT \int_{\mathrm{t-T}}^{t+T} dt'' A_x(t'') \int 2\pi i p^4 \sin^3\theta d\theta \\ \times \exp\left(2iI_{\mathrm{p}}T + ip^2T + \frac{\overline{\Delta_x^2}+\overline{\Delta_z^2}}{2} + ip\cos\theta\overline{\Delta_z}\right) \\ \times E_z^\star(t-T)E_z(t+T) \\ \times \mathbf{d}_z^\star[\mathbf{p}+\Delta(-T)]\mathbf{d}_z[\mathbf{p}+\Delta(T)] \\ = \int_{-\infty}^{\infty} dt A_x(t)\, G_2(t-\tau).\end{aligned} \tag{8.3}$$

$G_1(t)$ has the following expression:

$$\begin{aligned}G_1(t) = \int_{-\infty}^{\infty} dT \int 4\pi p^2 \sin\theta d\theta \left(1 + iTp^2\sin^2\theta\right) \\ \times \exp\left(2iI_{\mathrm{p}}T + ip^2T + \frac{\overline{\Delta_x^2}+\overline{\Delta_z^2}}{2} + ip\cos\theta\overline{\Delta_z}\right) \\ \times E_z^\star(t-T)E_z(t+T) \\ \times \mathbf{d}_z^\star[\mathbf{p}+\Delta(-T)]\mathbf{d}_z[\mathbf{p}+\Delta(T)].\end{aligned} \tag{8.4}$$

This is almost perfect barring the fact that G_1 still has few drive pulse related terms of the form, $\Delta_x(t') \coloneqq A_{\mathrm{x}}(t+t') - A_{\mathrm{x}}(t)$. The drive field is already very weak and if the response of the medium to this field is instantaneous, $\Delta_x(t') \to 0$. I numerical comparison confirms this. The drive pulse is neither energetic enough nor intense enough to cause any measurable contribution in the gating function that is not instantaneous.
For the second part, the additional integral over the vector potential of the drive pulse needs to be transferred to the gating function itself using variable transformation. The derivation, although simple, is long and not informative. I am only providing the final expression:

$$\begin{aligned}G_2(t) = \int 4i\pi p^4 dp \sin^3\theta d\theta \\ \times \left(\int_{\mathrm{t}}^{\infty} du E_z(u)\mathbf{d}_z[\mathbf{p}+\Delta_z(u)] e^{iu\left[I_{\mathrm{p}}+\frac{p^2}{2}\right]+\int_{-\infty}^{u} dt''\left[\frac{A_z^2(t'')}{2}+p\cos\theta A_z(t'')\right]}\right) \\ \times \left(\int_{-\infty}^{t} du E_z(u)\mathbf{d}_z[\mathbf{p}+\Delta_z(u)] e^{iu\left[I_{\mathrm{p}}+\frac{p^2}{2}\right]+\int_{-\infty}^{u} dt''\left[\frac{A_z^2(t'')}{2}+p\cos\theta A_z(t'')\right]}\right)^\star \\ +\text{c.c.}\end{aligned} \tag{8.5}$$

In conclusion, I have an analytical form of the gating function under the strong field approximation. Beyond the SFA itself, the only additional approximations that I made boil down to the assumption of how inert the drive field is in the entire excitation processes. Both in experiments and more involved simulations like tRecX, this assumption can be tested by checking for the linear response as predicted by Equation 4.4.

9. The Drift Current and the Gating Function of the Hydrogen Atom

Since all the results presented and discussed in part III of this thesis are about the hydrogen atom, I would like to dedicate this section to rewriting the equations for this specific medium. Everything remains the same except for the fact that I replace the placeholder **d** with the analytical dipole transition matrix element for ground state hydrogen. The equations for the drift current and the gating function in their most general forms are,

$$
\begin{aligned}
\langle -\hat{p}_x(\tau)\rangle = &-\int_{-\infty}^{\infty} dt \int_{-\infty}^{\infty} dT \int 4\pi p^2 dp \int \sin\theta d\theta \\
&\times \exp\left(2iI_{\mathrm{p}}T + ip^2T + \frac{\overline{\Delta_x^2}+\overline{\Delta_z^2}}{2} + ip\cos\theta\overline{\Delta_z}\right) \\
&\times \left(-A_x(t)J_0\left(ip\sin\theta\overline{\Delta_x}\right) + ip\sin\theta J_1\left(ip\sin\theta\overline{\Delta_x}\right)\right) \\
&\times E_z^{\star}(t-T)E_z(t+T)d_z^{\star}[\mathbf{p}+\Delta(-T)]d_z[\mathbf{p}+\Delta(T)], \\
G_1(t) = &\int_{-\infty}^{\infty} dT \int 4\pi p^2 dp \int \sin\theta d\theta \left(1 + iTp^2\sin^2\theta\right) \\
&\times \exp\left(2iI_{\mathrm{p}}T + ip^2T + \frac{\overline{\Delta_z^2}}{2} + ip\cos\theta\overline{\Delta_z}\right) \\
&\times E_z^{\star}(t-T)E_z(t+T)d_z^{\star}[\mathbf{p}+\Delta(-T)]d_z[\mathbf{p}+\Delta(T)], \\
G_2(t) = &\int 4i\pi p^4 dp \int \sin^3\theta d\theta \\
&\times \left(\int_{\mathrm{t}}^{\infty} du E_z(u)d_z[\mathbf{p}+\Delta_z(u)]e^{iu\left[I_{\mathrm{p}}+\frac{p^2}{2}\right]+\int_{-\infty}^{u}dt''\left[\frac{A_z^2(t'')}{2}+p\cos\theta A_z(t'')\right]}\right) \\
&\times \left(\int_{-\infty}^{t} du E_z(u)d_z[\mathbf{p}+\Delta_z(u)]e^{iu\left[I_{\mathrm{p}}+\frac{p^2}{2}\right]+\int_{-\infty}^{u}dt''\left[\frac{A_z^2(t'')}{2}+p\cos\theta A_z(t'')\right]}\right)^{\star} \\
&+ \text{c.c.}.
\end{aligned}
\tag{9.1}
$$

The dipole transition matrix element,

$$\mathbf{d}(\mathbf{p}) = \langle \mathbf{p} | \, e\mathbf{r} \, | n, l, m \rangle \,, \tag{9.2}$$

for a ground state $|1s\rangle$ to a plane wave $|\mathbf{p}\rangle$ transition [33] is

$$\Psi_{1\mathrm{s}}(r) = \frac{1}{\sqrt{\pi} a_0^{3/2}} e^{-r/a_0} \tag{9.3}$$

$$\implies \mathbf{d}(\mathbf{p}) = \frac{2^{7/2}(2I_\mathrm{p})^{5/4}}{\pi} \frac{\mathbf{p}}{\mathbf{p}^2 + 2I_\mathrm{p}} \tag{9.4}$$

Replacing this result in Equation 7.12, Equation 8.4, and Equation 8.5; I obtain:

$$\begin{aligned}
\langle -\hat{p}_x(\tau) \rangle = -\frac{2^9(2I_\mathrm{p})^{5/2}}{\pi} & \int_{-\infty}^{\infty} dt \int_{-\infty}^{\infty} dT \int\int p^2 dp \sin\theta d\theta \\
& \times \exp\left(2iI_\mathrm{p}T + ip^2T + \frac{\overline{\Delta_x^2} + \overline{\Delta_z^2}}{2} + ip\cos\theta\overline{\Delta_z} \right) \\
& \times \left(-A_x(t) J_0\left(ip\sin\theta\overline{\Delta_x} \right) + ip\sin\theta J_1\left(ip\sin\theta\overline{\Delta_x} \right) \right) \\
& \times E_z^\star(t-T) E_z(t+T) \cdot d(T) \cdot d(-T). \\
G_1(t) = \frac{2^9(2I_\mathrm{p})^{5/2}}{\pi} & \int_{-\infty}^{\infty} dT \int\int p^2 dp \sin\theta d\theta \left(1 + iTp^2 \sin^2\theta \right) \\
& \times \exp\left(2iI_\mathrm{p}T + ip^2T + \frac{\overline{\Delta_z^2}}{2} + ip\cos\theta\overline{\Delta_z} \right) \\
& \times E_z^\star(t-T) E_z(t+T) \cdot d(T) \cdot d(-T). \\
G_2(t) = \frac{2^9(2I_\mathrm{p})^{5/2}}{\pi} & \int\int ip^4 dp \sin^3\theta d\theta \\
& \times \left(\int_\mathrm{t}^{\infty} du E_z(u) d(u) e^{iu\left[I_\mathrm{p} + \frac{p^2}{2} \right] + \int_{-\infty}^{u} dt'' \left[\frac{A_z^2(t'')}{2} + p\cos\theta A_z(t'') \right]} \right) \\
& \times \left(\int_{-\infty}^{t} du E_z(u) d(u) e^{iu\left[I_\mathrm{p} + \frac{p^2}{2} \right] + \int_{-\infty}^{u} dt'' \left[\frac{A_z^2(t'')}{2} + p\cos\theta A_z(t'') \right]} \right)^\star \\
& + \text{c.c.},
\end{aligned}$$

where

$$d(\eta) := \frac{p\cos\theta + \Delta_z(\eta)}{(\mathbf{p} + \Delta_z(\eta) + \Delta_x(\eta))^2 + 2I_\mathrm{p}}. \tag{9.5}$$

I would like to point out that the Δ_x terms in the dipole moment are simply ignored so that the original assumption of linear interaction with the drive pulse to holds

true and the gating functions indeed end up being purely a function of the injection pulse. I have already argued that this should hold true if the changes caused by the drive potential are instantaneous in nature. It can also be checked numerically.

10. Approximations Involved in Obtaining Analytical Results

Very few Hamiltonians describing physical interactions are exactly solvable. In theoretical studies, one starts with a model, which by itself involves making a few justified approximations and assumptions. A model that describes everything correctly but cannot be used to obtain any useful information is not as useful as one that yields applicable results by only accounting for the most relevant physical dynamics. In my analytical approach, the first thing that is ignored is causality, i.e., the relativistic effects. These effects would become relevant once the field strength is so high that maximum kinetic energy of a free charge oscillating within the field, approaches the charge's rest mass energy: $2U_{\mathrm{p}} \rightarrow m_{\mathrm{e}}c^2$.
Another thing being ignored is the spatial variation of the optical field, under the dipole approximation. The dipole approximation indirectly allows ignoring the magnetic field of the optical pulse and remains valid [59, 60] until $\frac{U_{\mathrm{p}}}{2c\omega} < 1$.
The approximations mentioned are justified if one remains within the range of parameters where it is known that they do not play a significant role. In fact, even more 'exact' ab initio TDSE solvers also make these assumptions. The approximations I describe next are more drastic. These approximations are not present in exact numerical TDSE solvers, but these packages are often designed to emulate these approximations, when needed, for comparisons and benchmarking.
The most drastic assumption made under the SFA model is the usage of the Volkov states as the continuum state. An electron in the Volkov state will remain uninfluenced by the Coulombic potential. In reality, a linearly polarized pulse can accelerate the electron back towards the atom to experience '**recollision**', where it achieves energies far beyond what the AC electric field would have been capable of alone. As such, SFA can under-predict the outgoing momentum of the electron. As an analogy I would like to remind the reader of the gravitational slingshot effect [61] used to accelerate objects using a planet's gravitation potential. Using SFA is akin to the planet disappearing once the space-shuttle exceeds the terminal velocity. The optical field acts like the space-shuttle's jets and the ionized atom as the planet. Without the planet (ion) even if the jets (optical field) were configured to sling-assist (recollide and accelerate) the space-shuttle (electron) cannot be accelerated further away.

Another thing being ignored is the change in the ground state itself. As more electrons get ionized, the cross-section of available ionizable electrons reduces. For a single atom, a similar effect would occur with an increasing portion of the electron wave packet being in the Volkov state instead of the ground state. This '**depletion**' is not considered in my model. It could be accounted for classically by obtaining the result for several atoms and then normalizing the results, but that is still not a full quantum-mechanical treatment that would consider how the lack of electrons affects the ground state itself.
SFA can be extended to have additional ionization channels, but my model only considers direct, ground state to continuum, transitions. Changes caused due to resonances [62] with intermediate bound states are not accounted for.
Though not an approximation, the gauge choice affects the results. All my derivations start with the SFA model the hydrogen atom in the length gauge. The idea of gauge invariance is only valid in an approximation free case. With any perturbative expansion, the results obtained from the equations as well as the possible physical interpretations of those equations change with gauge.
There is a detailed overview [63] of the physics that is not captured by SFA for photoionization from ultrashort pulses, especially when the quantity being inspected is related to the angular distribution of the photoionized electron. On top of the approximations involved in SFA, I also needed some additional approximations to obtain the final form of the gating function that could be interpreted as the ionization rate.
First, whenever useful, I ignored $\mathbf{E}_{\text{drive}}$ in expressions involving its sum with $\mathbf{E}_{\text{inj}}$. In NPS this is justified since $E_{\text{drive}} \ll E_{\text{inj}}$, In LPS, where the amplitudes of the two fields are comparable, this approximation still works because the injection field has frequency components that allow the existence of a stationary phase, making other contributions less relevant. For obtaining the delay dependent drift current, this meant assuming

$$(\mathbf{E}_{\text{inj}} + \mathbf{E}_{\text{drive}}) \cdot \mathbf{d}[\mathbf{p} + \Delta_{\text{drive}} + \Delta_{\text{inj}}] \approx \mathbf{E}_{\text{inj}} \cdot \mathbf{d}[\mathbf{p} + \Delta_{\text{drive}} + \Delta_{\text{inj}}]$$

in Equation 3.8 for the continuum wave function of the electron.
Additionally, to truly make the gating function independent of the drive field, a similar approximation was used for the terms inside the dipole transition matrix elements

$$\mathbf{d}[\mathbf{p} + \Delta_{\text{drive}} + \Delta_{\text{inj}}] \approx \mathbf{d}[\mathbf{p} + \Delta_{\text{inj}}]$$

and for a term in the phase where

$$\Delta_{\text{drive}}^2 + \Delta_{\text{inj}}^2 \approx \Delta_{\text{inj}}^2.$$

I justified this approximation on the grounds that the drive field is weak enough that only has instantaneous interactions making $\Delta_{\text{drive}} = \mathbf{A}_{\text{drive}}(t+t') - \mathbf{A}_{\text{drive}}(t) \to 0$ and by checking if the numerical results remain unchanged.
Second, to obtain the gating function, I expanded the Bessel functions

$$J_0(ip\sin\theta\overline{\Delta_x}) = 1 - \left(\frac{ip\sin\theta\overline{\Delta_x}}{2}\right)^2 + \ ....$$
$$J_1(ip\sin\theta\overline{\Delta_x}) = \frac{ip\sin\theta\overline{\Delta_x}}{2} - \frac{1}{2}\left(\frac{ip\sin\theta\overline{\Delta_x}}{2}\right)^3 + \ ...$$

considering only the zeroth order terms.
Beyond this, numerical integration itself is an approximation. A digital computer cannot integrate over a continuous axis and needs the user to define a meaningful discretization such that

$$\int f(x)dx \approx \sum_{\text{x}\in\text{X}} f(x).$$

By increasing the grid density until the results stop changing in values and converge, this approximation can be ignored for most parts. It only sets limitations on what can be computed numerically. As an example, the number of points required to resolve the extensive range of electron momenta resulting from an extremely high intensity injection pulse are simply too numerous to yield converged numerical results.

Part III.

Results and Discussions

11. Linear Photoconductive Sampling

Having presented all the relevant theoretical background for numerically simulating photoconductive sampling under the strong field approximation, I shall now proceed with the actual plots and their respective comparisons with tRecX simulations. As I had briefly explained in chapter 4, LPS is usually done first before moving on to the nonlinear case. The motivation behind this chronology is quite simple— there are fewer unknown variables involved in linear interactions. The injection pulse is defined such that all its photons have are more energetic than the ionization potential. This ensures pure linear charge injection. If the FWHM of the injection pulse is short enough, the plot of the current will coincide with the vector potential of the drive pulse, up to a constant factor. This is not as interesting as the gating functions. Owing to the relative simplicity of the injection process, I will directly present the gating function for LPS, obtained from SFA.
Before proceeding, I would like to modify Equation 8.5.
I make the rotating wave approximation (RWA) [64]. It is often employed for near resonance transitions between multi-level systems, atoms etc. I will make the following replacement in Equation 2.1:

$$\mathbf{E}(t) = \frac{\xi(t)e^{i\omega_c t} + \xi^\star(t)e^{-i\omega_c t}}{2} \approx \xi(t)\frac{e^{-i\omega_c t}}{2} := \mathbf{E}^{\mathrm{RWA}}(t).$$

RWA is considered a valid approximation as faster oscillations have negligible contributions. This is not the case for G_2. RWA ensures that the phase of the integral in G_2 never exceeds the ionization threshold. In LPS only single photon transitions that are caused by low intensity light fields occur. This is the ideal case for using RWA and experimental results support that [65]. With this the second

gating function (Equation 8.5) becomes:

$$
\begin{aligned}
G_2^{\mathrm{RWA}}(t) = \int & i\pi p^4 dp \sin^3\theta d\theta \\
& \times \left(\int_{\mathrm{t}}^{\infty} du \xi_z(u) \mathbf{d}_z[\mathbf{p} + \Delta_z(u)] e^{-i\omega_{\mathrm{c}} u + iu\left[I_{\mathrm{p}} + \frac{p^2}{2}\right] + \int_{-\infty}^{u} dt'' \left[\frac{A_z^2(t'')}{2} + p\cos\theta A_z(t'')\right]} \right) \\
& \times \left(\int_{-\infty}^{t} du \xi_z(u) \mathbf{d}_z[\mathbf{p} + \Delta_z(u)] e^{-i\omega_{\mathrm{c}} u + iu\left[I_{\mathrm{p}} + \frac{p^2}{2}\right] + \int_{-\infty}^{u} dt'' \left[\frac{A_z^2(t'')}{2} + p\cos\theta A_z(t'')\right]} \right)^{\star} \\
& + \text{c.c.}
\end{aligned}
\tag{11.1}
$$

As apparent in Figure 11.1, equations with the RWA (red) result in a smooth gating function, but without it(green), my model predicts fast oscillations.
The weak injection pulse used for linearly exciting the electron contain photons with energies that exceed the ionization potential (band gap in solids). For such pulses, the electric field oscillates very quickly between the local maxima, minima, and null field. This in turn could imply that the ionization process too can have fast oscillations. However, in photoconductive sampling, the gating function is first the result of deconvolution, and then a representative of the ionization process. Since the drive pulse cannot be more energetic than the ionization potential itself, all frequency components of the gating function that exceed the ionization threshold are not observable and must be discarded.
I could have removed the higher frequency components numerically. However, it is better to avoid such frequency filtering and changes to the original analytical expression that have the same end-result also provide insights into the physical source of the oscillations.
The ultrafast oscillations could still be relevant if the gating function is a valid ionization rate model in a different experimental set-up. The analytical approach hints at a possible limitation of RWA. Even for a single photon photoionization process, a case where RWA works the best, there still are some fast phenomena that RWA cannot capture.

Figure 11.1 confirms an already well-known notion: when photoionization is caused by individual photons of the light pulse, the ionization rate is simply a function of the intensity pulse envelop of the optical field.

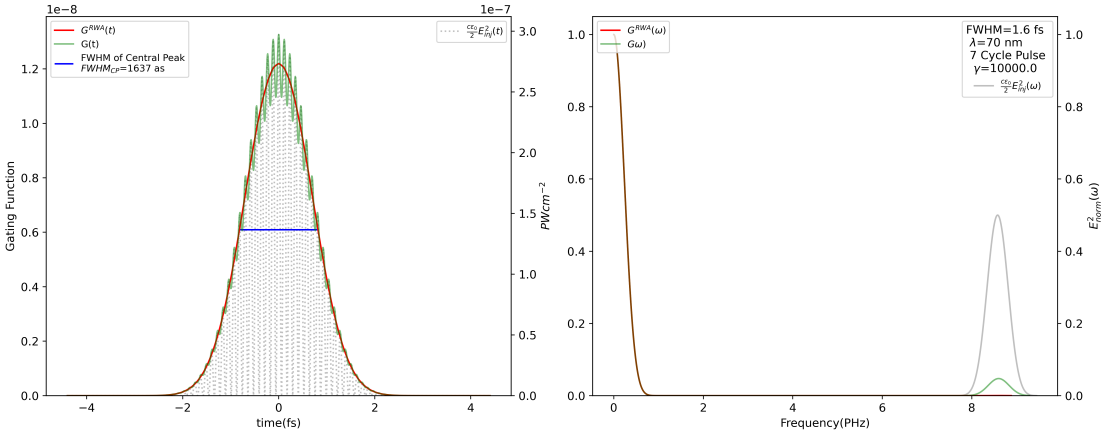

Figure 11.1.: Gating Function of an Injection Pulse that used for LPS. The curves compare the square of the injection field with the gating functions both with and without RWA.

12. Nonlinear Photoconductive Sampling

The LPS results discussed in chapter 11 indicate that my analytical results can capture the physics observed in the experimental setup. As mentioned in chapter 4, LPS is only the first step. It demonstrates that it is possible to recover the optical field using photoconductive sampling. The true technological leap requires exploiting nonlinear interactions, which enable sub-cycle photoinjection. The time during which a sample becomes conductive can be much shorter than the actual duration of pulse.

In chapter 7, I obtained an equation that allows me to directly compute the gating

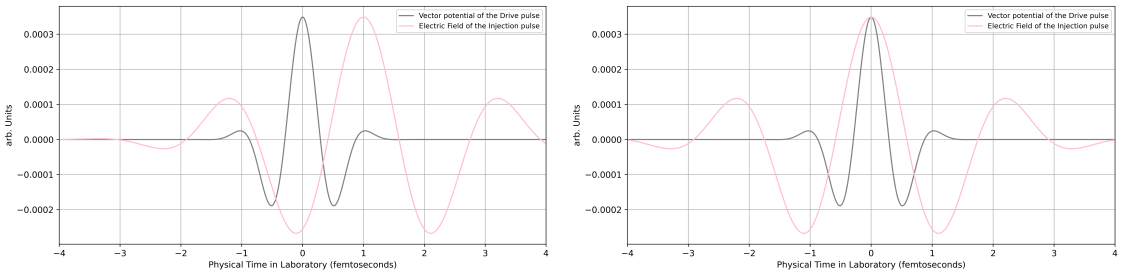

(a) delay $\tau = 1$fs (b) delay $\tau = 0$fs

Figure 12.1.: Pulses as defined in simulations. The peak intensity of the drive pulse remains static while the injection pulse is moved around. The defined convolution allows comparing the vector potential and drift current easily. In a delay scan, a positive delay corresponds to the physical case of the injection pulse arriving after the drive pulse.

function. With some further simplification I obtained Equation 9.5 specifically for the hydrogen atom. Unlike LPS, the form of the gating function involved in NPS is more complicated. Even if the exact injection and drive pulses were known, deconvolution of the delay dependent current can be ambiguous for such a complex gate. Multiple functions will yield the same delay-dependent drift current for a given drive pulse. For this reason, I will limit myself to comparing delay dependent $p_{\mathrm{x}}(\tau)$ as obtained from tRecX and SFA.

Unlike LPS, where only the central wavelength is of relevance, both the intensity and the wavelength play a role in shaping the nonlinear interactions involved in NPS. Since three-dimensional plots are cumbersome, it is useful to have a parameter that can quantify both wavelength and the intensity to define the relative strength of light field. As mentioned in chapter 2, Keldysh used a unitless quantity to parameterize his equations. It is defined as

$$\gamma_{\mathrm{K}} = \frac{c\sqrt{2mI_{\mathrm{p}}}}{2\pi\lambda \cdot e \cdot |\mathbf{E}(t)|}.$$

As mentioned in chapter 3, γ_{K} can be used to distinguish between regime whether quasi-static tunneling, or the multi-photon ionization take precedence. Before presenting any results, I would like to bring Figure 12.1 to the reader's attention. It portrays how the drift current is obtained for a given delay. It clarifies the interpretation of the x-axis for all subsequent results that I will present. A positive delay corresponds to the peak of the injection pulse (and thereby the duration when most photoionization occurs) arriving after the peak of the drive pulse.

12.1. Comparison with Quasi-Static Tunneling Ionization Rates

As I had discussed in subsection 3.1.1, when the field strength is increased beyond a certain point, it becomes possible to describe the ionization process using a semi-classical tunneling model. The AC field of the optical pulse behaves like a DC field in that only the ionization rate is purely determined by the absolute value of the instantaneous electric field. I had also provided Equation 3.1, the ADK formula, as a simple model quantifying this idea.
Using Equation 3.2, I can calculate the quasi-static tunneling ionization rate. Since I know the field at any given time for $E_{\mathrm{inj}}(t)$, I can plot $W_{\mathrm{H,1s}}(E_{\mathrm{inj}}(t))$ and compare it with the gating function $G(t)$. For ease of presentation, I will normalize everything and mention $\frac{W_{\mathrm{max}}}{G_{\mathrm{max}}}$.

As a sanity check, I compare my gating function with the ionization rate for $\gamma_{\mathrm{K}} \approx 1.4$, corresponding to a field intensity where the quasi-static approach is invalid. In Figure 12.3 the gating function ($G(t)$, blue) and the tunneling ionization rate($w(E(t))$, orange) look quite different. The scatter plot for the gating function with respect to the instantaneous field has multiple values for the same $|E|$. This is a clear indication that ionization is no longer quasi-static, i.e., not a direct function of the absolute value of instantaneous field.

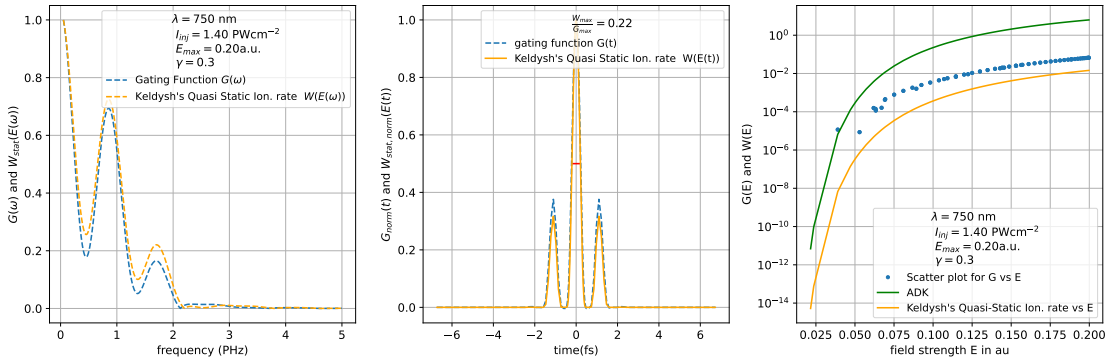

Figure 12.2.: Comparison of the gating function with quasi-static ionization-rate based results. The field with $I = 1.4$ PW cm^{-2}, and $\gamma_K = 0.3$ is in the quasi-static regime. Both ADK and Keldysh's quasi-static tunneling ionization rates are included for Rate vs Field plot.

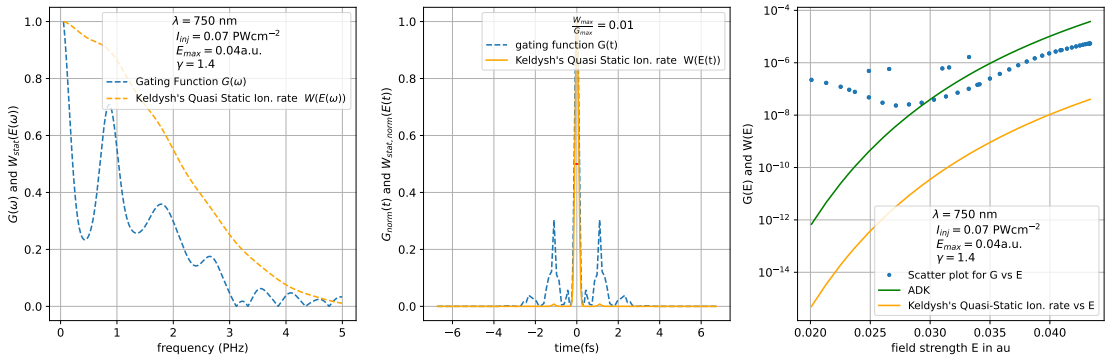

Figure 12.3.: Comparison of the gating function with quasi-static ionization-rate based results. The field at 0.066 PW cm^{-2} is far too weak for quasi static tunneling model to be valid.

12.2. Comparison with tRecX

Jumping right into it, Figure 12.4 presents a promising future for SFA. The results seem to match qualitatively with the ab initio results. In tRecX, higher current is predicted during the secondary half-cycles of the drive pulse. Interactions like atom polarization and recollision can easily cause this.

Figure 12.5 shows a case where the intensity of the injection pulse is decreased while everything else remains unchanged from Figure 12.4. There definitely are discrepancies worth discussing. The first thing to notice is that there is a lack of symmetry in the tRecX results. This would suggest that the half cycle corresponding to the local minimum of the injection pulse shown in Figure 12.1b that occurs around

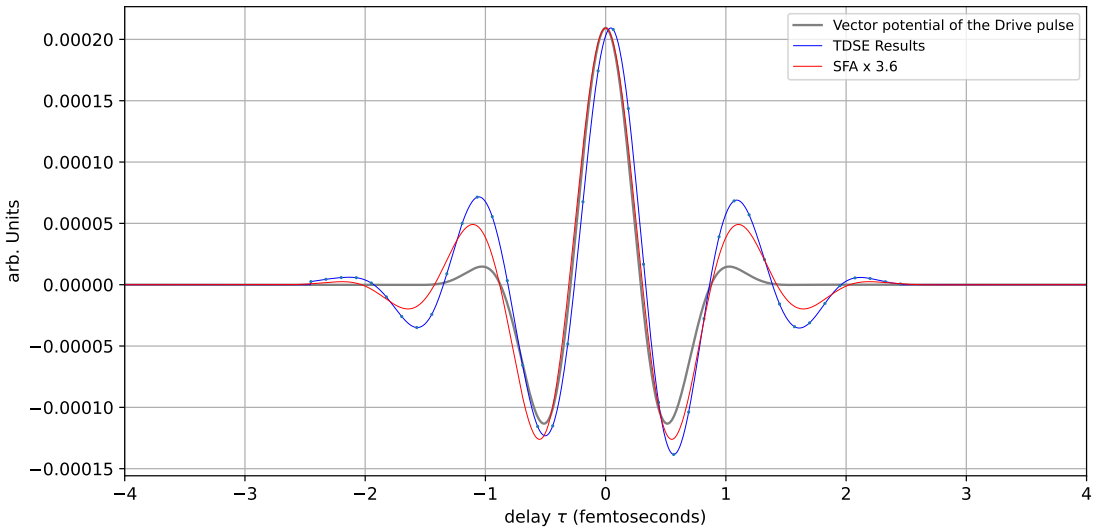

Figure 12.4.: $p_x(\tau)$ obtained from tRecX(blue) and SFA(red). Intensity $I_{\text{injection}} = 0.4$ PW cm^{-2}, Wavelength $\lambda = 750$ nm, Keldysh Par. $\gamma_K = 0.57$

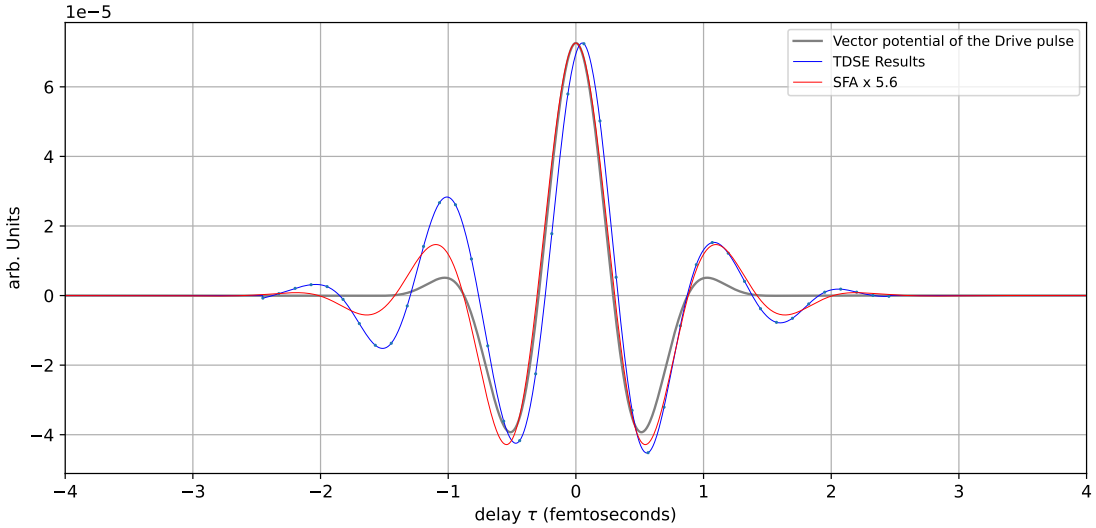

Figure 12.5.: $p_x(\tau)$ obtained from tRecX(blue) and SFA(red). $I_{\text{injection}} = 0.25$ PW cm^{-2}, Wavelength $\lambda = 750$ nm, Keldysh Parameter $\gamma_K = 0.72$

one femtosecond ionizes more than what SFA predicts. To support the idea that it indeed is the third peak causing this discrepancy, I present Figure 12.6, where I modified the gating function to make the third instance of ionization larger than one predicted by SFA. Interpreting the results more directly; when the drive pulse

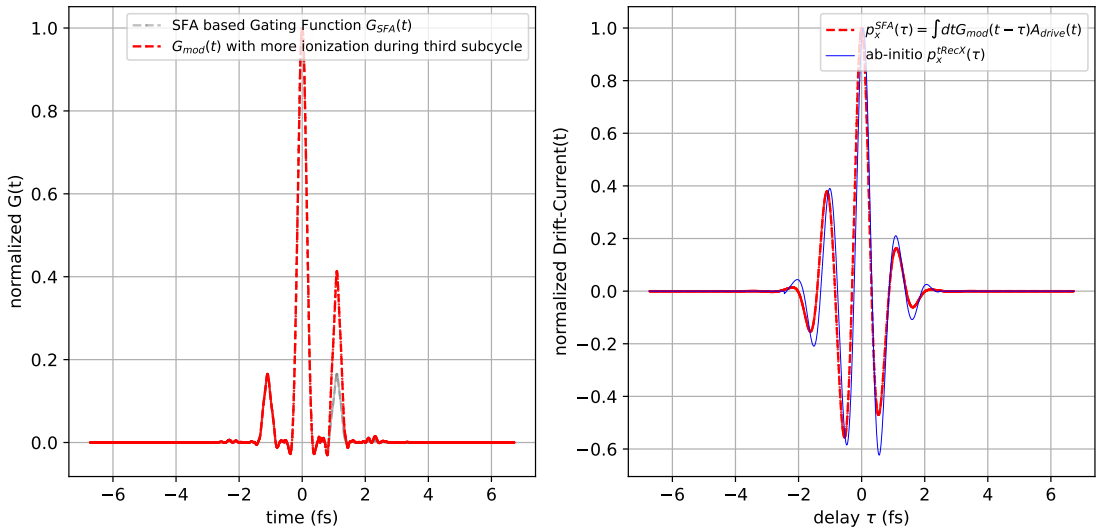

Figure 12.6.: Comparison of SFA and tRecX results. The gating function obtained using SFA is modified to smoothly increase the net ionization that occurs during the third sub-cycle of the injection pulse. When the modified fating function is used, the delay-dependent drift current becomes qualitatively similar. Like Figure 12.5, $I_{\text{injection}} = 0.25$ PW cm^{-2}, Wavelength $\lambda = 750$ nm, Keldysh Parameter $\gamma_{\text{K}} = 0.72$

arrives after the injection pulse, the net drift of electron in the direction of the drive field is more than one might expect. The event in question involves multiple photons from two orthogonal pulses with vastly different intensities, central wavelengths, and durations. Pinpointing the cause of this discrepancy is hard as there are many culprits.

Is there a mechanism that can change the ground state hydrogen atom over time? Existing literature hints at the possibility that laser-dressed bound states can cause this. For a given intensity, resonant multi-photon ionization by itself can cause both a reduced and an increased ionization probability [66]. As shown in [67] a reduction in ionization probability is caused by the electron being excited to a stable bound state rather than the continuum. Given enough time, such a state should relax back to the ground state. However, the pulses in question are so short that new photons, either from the injection or the drive pulse, arrive before any relaxation can occur and directly excite the electrons from the bound state to the continuum. This effect has not been discussed in depth in existing literature. It was reported that semi-classical SFA is indeed unable to capture the quantum mechanical changes in the angular distribution of the momentum [63]. The bound states are closer to the continuum so, when compared to ground-continuum transitions, bound-continuum

transitions require fewer photons of the same pulse. A new ionization channel is available that would also work with lower intensities. For example, one photon of a single cycle 750 nm pulse (1.65 eV) is sufficient for direct transitions from the third orbital (-1.51 eV) to the continuum. Two photons of the same pulse are sufficient for transitions from the second orbital. It could increase the magnitude of ionization rate, like in Figure 12.6. It could also broaden the third peak by making ionization occur at much lower intensities. The observations made in Figure 12.5 can be explained by either of the two.

To test my hypothesis, I employ toy models. If bound states are indeed behind the discrepancy, eliminating their presence should remove it. The way I go about it is by modifying the Hamiltonian of the hydrogen atom in tRecX. Usually, the Coulombic potential is truncated at 60 atomic units. This allows for easier calculations, since there truly is no potential beyond that point, leaving simpler equations. Convergence tests confirm that it does not affect the observable in question. Even when this truncation point is moved all the way to two hundred atomic units the results remain unchanged. Now, instead of defining the truncation to be realistic, I define it to remove the excited bound states while leaving the ground state unaffected. At a user-defined point A, the Coulomb potential drops exponentially, becoming zero at another user-defined point B. The choice is made such that over ninety-nine percent of the electronic density in the ground state remains within the sphere defined by $|\mathbf{R}| = A$. Thus, I can be sure that only the excited states of the hydrogen atom are affected by this.

Figure 12.7 supports my hypothesis very strongly. As discussed in its caption, the presence of bound states, or lack thereof, has a significant effect on the delay-dependent drift current and just the first and the second excited states are sufficient to increase the total fraction of the atom ionized and to have a mechanism that can result in an asymmetric ionization despite a symmetric injection pulse.

In a certain sense, the hydrogen atom is the simplest case of strong-field ionization. The static Hamiltonian is exactly solvable and there are no many-body interactions to pay heed to. Still, as is clear from the results I have presented so far, it can be extremely complicated. Even here, the number of suspects that could cause the discrepancies I observe are not limited to the two I discussed. Systematically ruling out every single candidate is beyond the scope of my thesis. I believe that it can be a source of future investigation. To the best of my knowledge, existing literature underplays the role of the bound states and I hope that my results, which suggest the contrary, will motivate more people to investigate it.

I would like to remind the reader of the primary aim of my theoretical foray into strong field excitation in the hydrogen atom. The analytical equations I obtained lay a rigorous quantum mechanical foundation for photoconductive sampling. SFA is a well-tested theory and the results differing from tRecX simulations is a moment

to rejoice as it indicates the existence of physical effects that might not have been that well studied. I will discuss this in detail at the end of the next section. Here, it suffices to remember that even when the results from the strong field approximation do not conquer with the ones from tRecX, the SFA results stand on their own and a lot of useful information can be extracted from the analytical gating function obtained from SFA.

12.3. Detailed Inspection of the Gating Function

The analytical equations obtained for the gating function are extremely useful by themselves. Even if the SFA cannot clarify the finer details of strong-field ionization, it provides deep insights into the basic mechanism by which electrons are liberated from the atomic potential and measured in pump-probe setups. All experimental pump-probe setups will have additional physics not captured by SFA that is unique to them. Those problems need to be solved per case. However, the results from SFA can act as a good starting point for further investigations.
Photoconductive sampling is a technique, not an experiment. Discrimination is necessary as, unlike an experiment, a technique aims to have broad applicability. As a technique to obtain field resolved measurements, the aim is to have the broadest bandwidth, that is, ability to resolve the light signature of as slow and as fast physical phenomena as possible. In time domain, this means limiting the instance of ionization to a delta-like peak. The same thing can be viewed in the frequency domain via a simple Fourier transform of the gating function. Here, the ideal gating function will have a smooth Gaussian peak centered at zero, extending to high frequencies.
With this preamble, I present the first series of plots (Figure 12.8a, Figure 12.8b, Figure 12.9a, and Figure 12.9b). Detailed discussion has been delegated to the captions of for clarity and to avoid redundancy. The plots try to show the duration of the central ionization events by reporting its FWHM.
The main conclusion that can be made based on the information using Figure 12.8a, Figure 12.8b, Figure 12.9a and Figure 12.9b is that for nonlinear photoconductive sampling, there exists an ideal intensity when the gating function is as close to the ideal case as theoretically allowed. For all higher intensities, the duration of the main ionization event is longer, and the relative contribution made by secondary ionization events increases. While lowering the intensity further, can reduce the ionization duration, the scaling is not linear and at some point, the signal produced will simply be too weak to warrant the additional small gain in time-resolution. It is highly likely that a more exact quantum mechanical model will confirm this

fact. The value of this ideal intensity for the injection pulse might change but the idea that there is a range where multi-photon ionization and tunneling ionization balance each other out in a manner that minimizes ionization duration should still be applicable. Usually, the intensity of the pulse is the easiest to change. For a given central wavelength, an experimentalist employing photoconductive sampling and other similar techniques should try tuning the intensity as it is the path of least resistance to obtain better resolution. Even more nuance is added to this observation when the central wavelength is changed. A shorter central wavelength, i.e., a higher central frequency corresponds to an increase in the availability of more energetic photons. Unlike intensity, the central wavelength imposes more fundamental restrictions on nonlinear processes. The energy required to make a medium conductive— band gap in solid and ionization potential in atoms— does not change. For shorter wavelengths, the number of photons required to reach this threshold energy decreases since the individual photons participating in the interaction are more energetic. This would imply that the degree of nonlinearity decreases with decreasing central wavelength. This still needs to be confirmed by the plots of the gating function. I again present a series of figures (Figure 12.10a, Figure 12.10b, Figure 12.11a, and Figure 12.11b) to hint at a general trend when it comes to changing wavelengths. The Keldysh parameter remains unchanged. The individual cases can be tuned to achieve shorter injection durations, but the difference between the FWHM of the central peak of the three figures is large enough to be indicative of the general trend.

Based on the preceding group of images, I conclude that reducing the wavelength allows shorter injection duration. The trade-off is that the secondary peaks become more dominant. This can be circumvented if the FWHM of the injection pulse is less than one cycle as that directly reduces the intensity of the secondary sub-cycle maxima of the light field.

To conclude this discussion, I present Figure 12.12. Once the results from Figure 12.12 are available, a lot of conclusions start becoming obvious. For a single cycle pulse, **a shorter central wavelength** is physically shorter. So individual **sub-cycle spikes are narrower**. So, the injection duration for NPS performed with shorter central wavelength is shorter. It should be noted that a less energetic, i.e., longer wavelength, injection pulse still limits the ionization events to a smaller part within its cycle as shown in Figure 12.13. This feels obvious now, but I would like to emphasize that I could provide the intuitive argument only after I had obtained the gating function over a vast parameter domain. After seeing all the results, it seems intuitive that beginning from tunneling ionization, decreasing the intensity shortens the injection duration, since a smaller part of optical pulse achieves field strengths exceeding a "cut-off" value to initiate tunneling. This reduction with peak intensity is not linear and is lower bound by the multiphoton ionization processes

taking over. All these conclusions, although intuitive are not obvious and to the best of my knowledge the relation between injection-duration, intensity and wavelength has rarely been discussed in the literature. These results are especially useful for any technique that wants to exploit nonlinear light matter interaction to create ultra-fast ionization events (like TIPTOE and NPS).

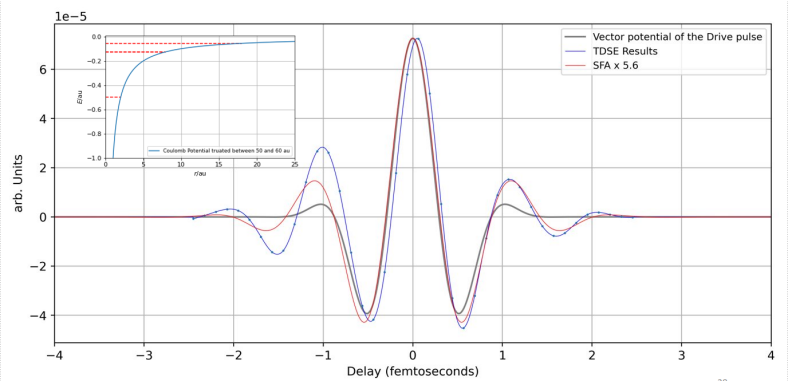

(a) Coulomb potential of the H atom

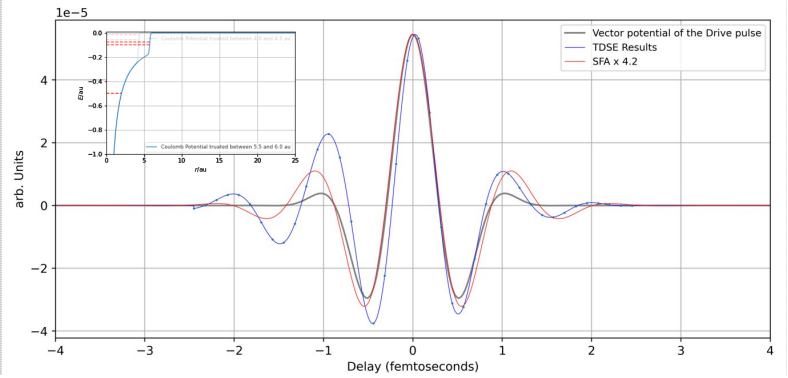

(b) Truncated leaving GS unperturbed

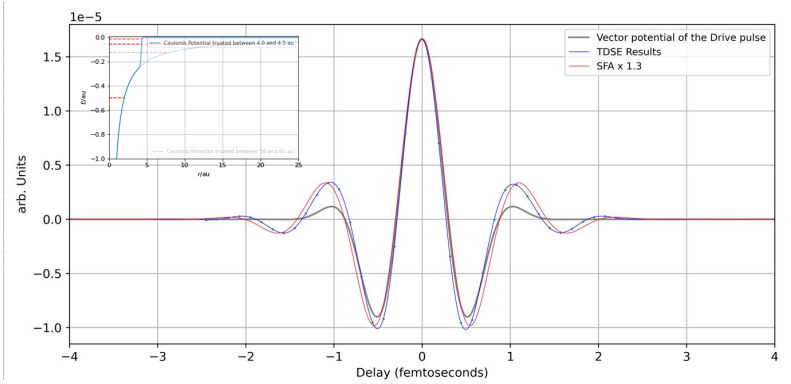

(c) Truncation even closer to nucleus. The ground state is still unperturbed

Figure 12.7.: Subplots **a**, **b** and **c** show the delay dependent drift current obtained with a Coulomb potential, modified as shown in their respective insets. **a** simply has the real hydrogen atom. **b** is an aggressive truncation, but the 1st and 2nd excited states are still far from the continuum. **c** is truncated only 1.5 au closer to the nucleus than **b** but the excited states are very close to the continuum.

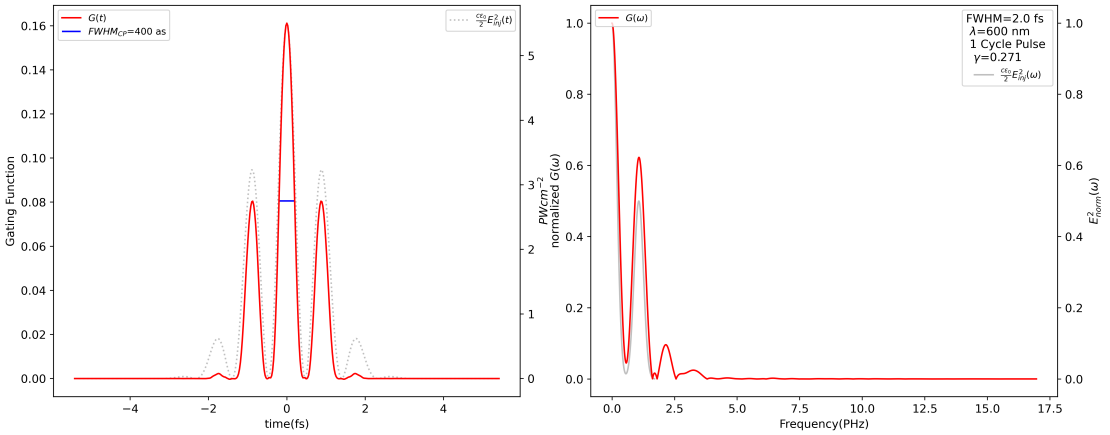

(a) Gating Function produced by an injection pulse with an FWHM of one cycle (2 femtoseconds). $\gamma_K = 0.27$. This would indicate that the intensity is high enough that the electric field of the injection pulse bends the Coulomb potential and lowers the potential barrier to an extent that electrons reach the continuum primarily by tunneling. The ionization process is limited to three instances. The secondary peaks in the time domain are almost half as large as the main central peak. This is not ideal. It is also apparent in the frequency domain, where the local minima and maxima are significantly different. It would mean that different frequency components of the drive pulse will be weighted differently by a significant margin. The FWHM of the central ionization event is 400 attoseconds.

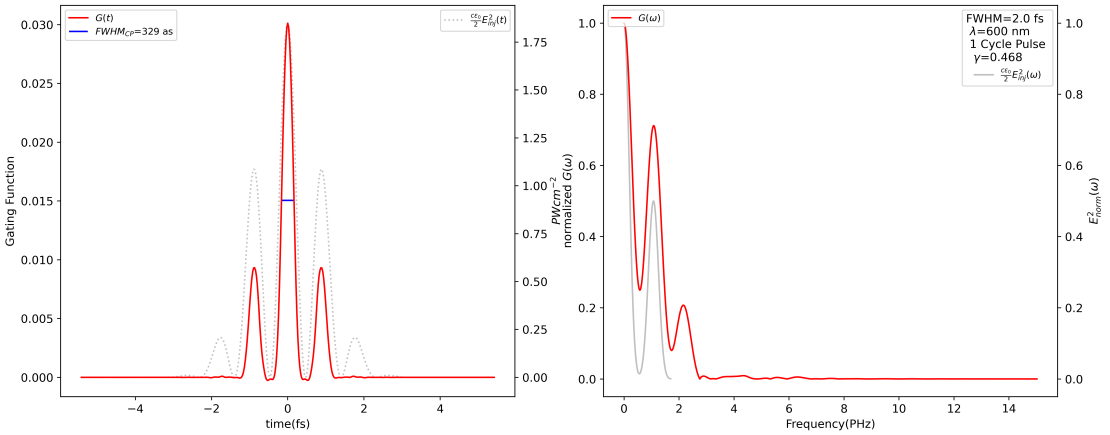

(b) Gating function of a single cycle 600 nm pulse with $\gamma_K = 0.47$. The intensity is still high enough that electrons are primarily ionized via tunneling. There still are three ionization events but the secondary peaks are significantly weaker. A smaller part of the injection pulse achieves the 'cut-off' intensity. In frequency domain, the local minima and maxima differ less, and the curve extends to higher frequencies. The FWHM of the central ionization event is 351 attoseconds, an improvement over the previously presented 329 attoseconds.

Figure 12.8.: Comparison of gating functions produced by pulses of different intensities

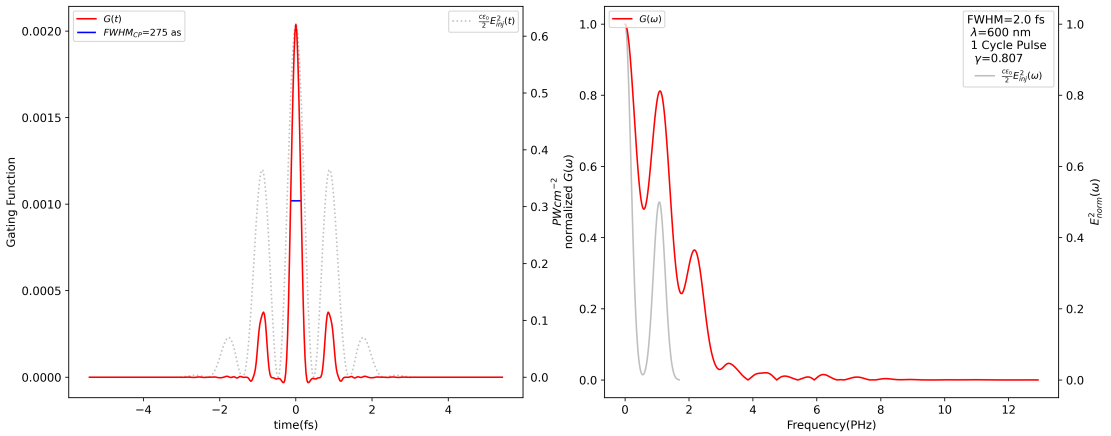

(a) Gating function of a single cycle 600 nm pulse with $\gamma_K = 0.81$. The ionization process seems to be even more localized than the previous two cases, with small secondary peaks and FWHM of just 275 fs

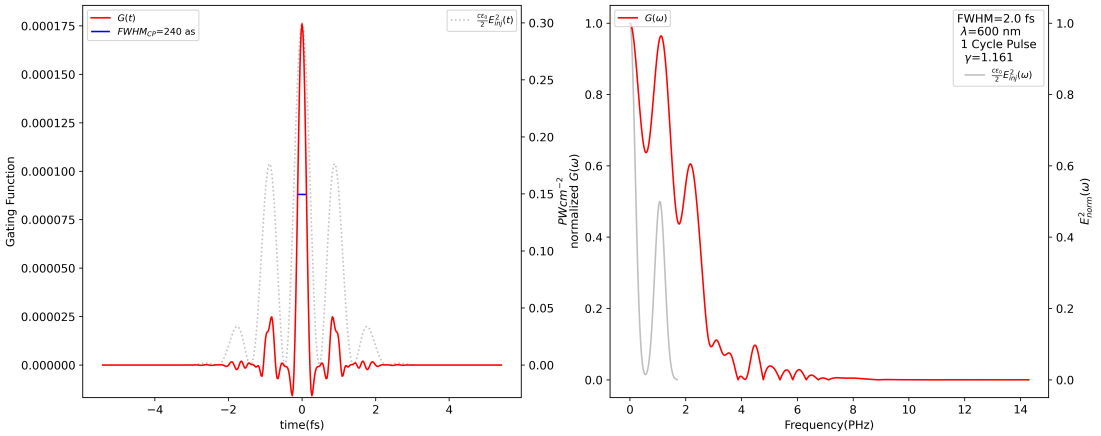

(b) Gating function of a single cycle 600 nm pulse with $\gamma_K = 1.161$. It is already at the limits at what may be numerically computed. The FWHM of the central ionization event is shorter than when $\gamma_K = 0.81$ at 240 fs. As I will discuss later, this indicates diminishing returns. Reducing the intensity generally reduced the ionization duration but not linearly. Combined with less net ionization occurring to overcome background noise this would place a limit on how low of an intensity is fruitful for experimental setups.

Figure 12.9.: Comparison of gating functions produced by pulses of different intensities

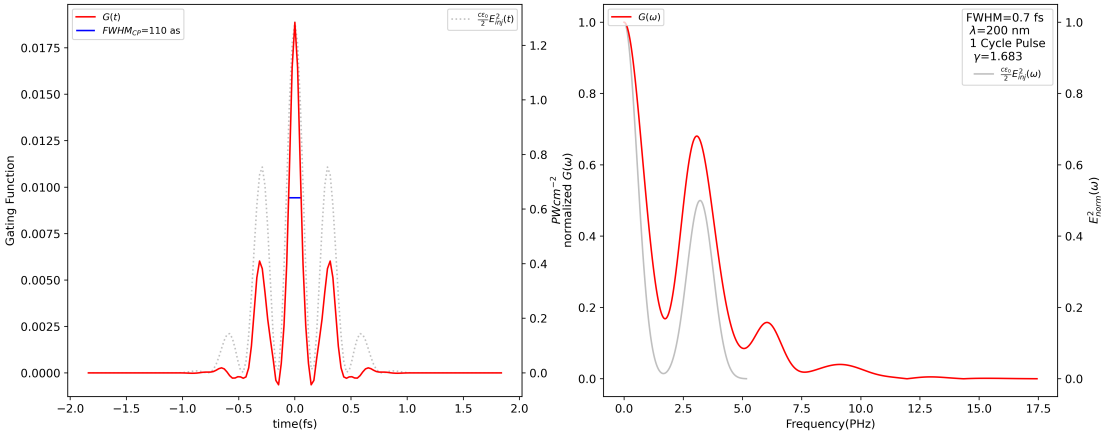

(a) 200 nm

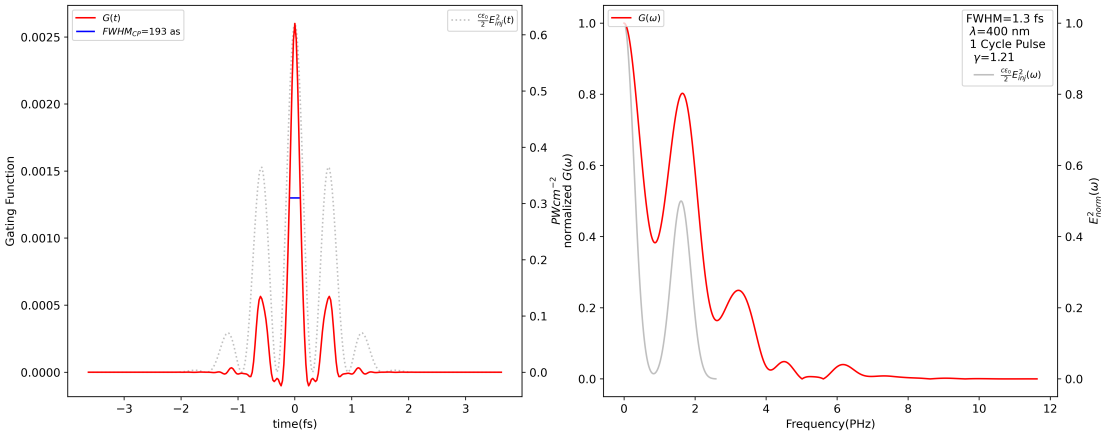

(b) 400 nm

Figure 12.10.: Comparison of gating functions produced by pulses of central wavelengths 200 nm and 400 nm.

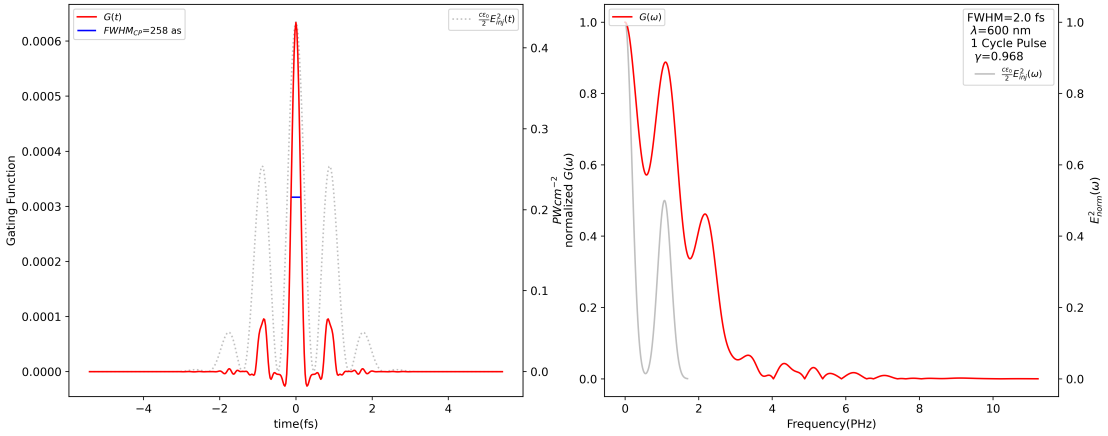

(a) 600 nm

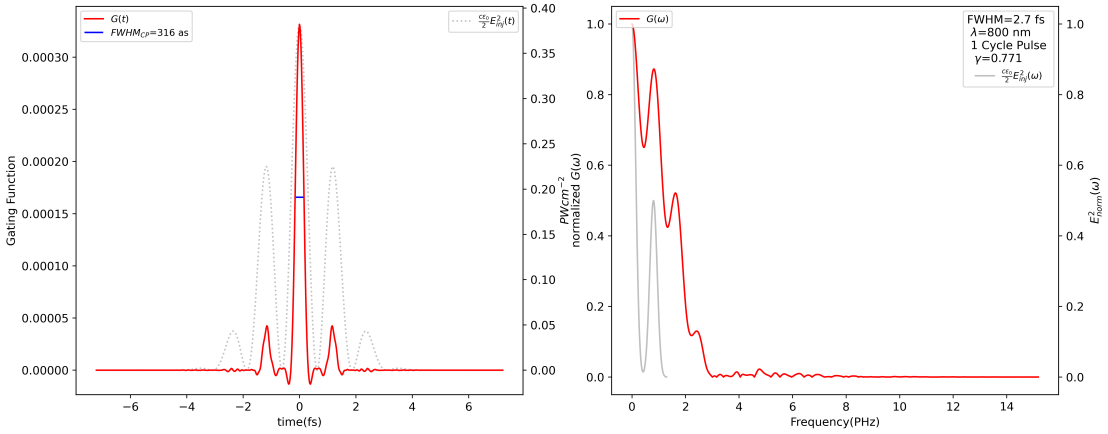

(b) 800 nm

Figure 12.11.: Comparison of gating functions produced by pulses of central wavelengths 600 nm and 800 nm.

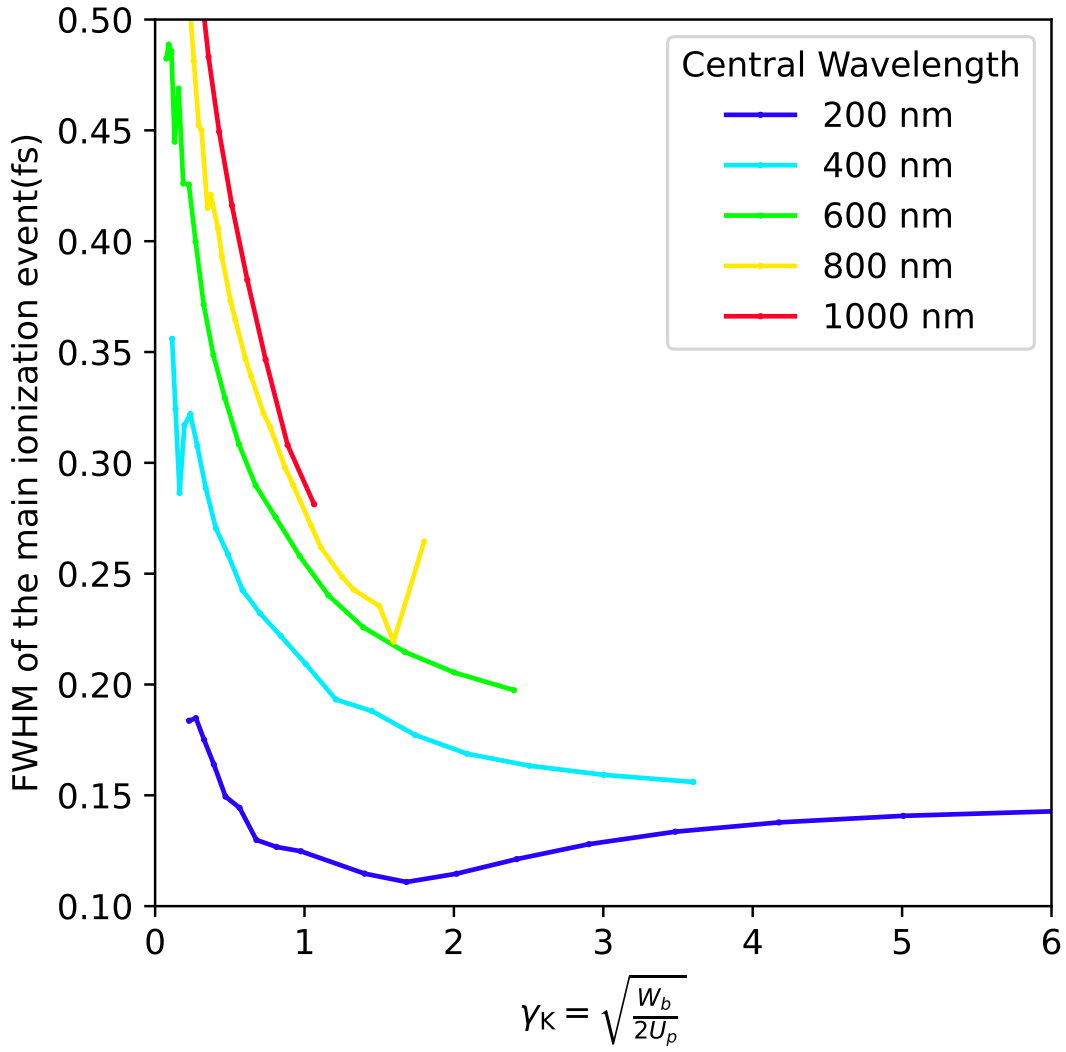

Figure 12.12.: A plot that tries to summarize the effect on injection duration when tuning both the central wavelength and the intensity. The x axis is the **Keldysh parameter** while the y axis is the FWHM of the central ionization event in **femtoseconds**. This parameter does not capture the presence of additional ionization events, but they may be ignored by arguing that it is possible to produce sub-cycle pulses. Distinct colors portray the different central wavelengths. Shorter wavelengths allow shorter ionization duration but with diminishing returns as is visible from the curves getting increasingly flatter with decreasing wavelength.

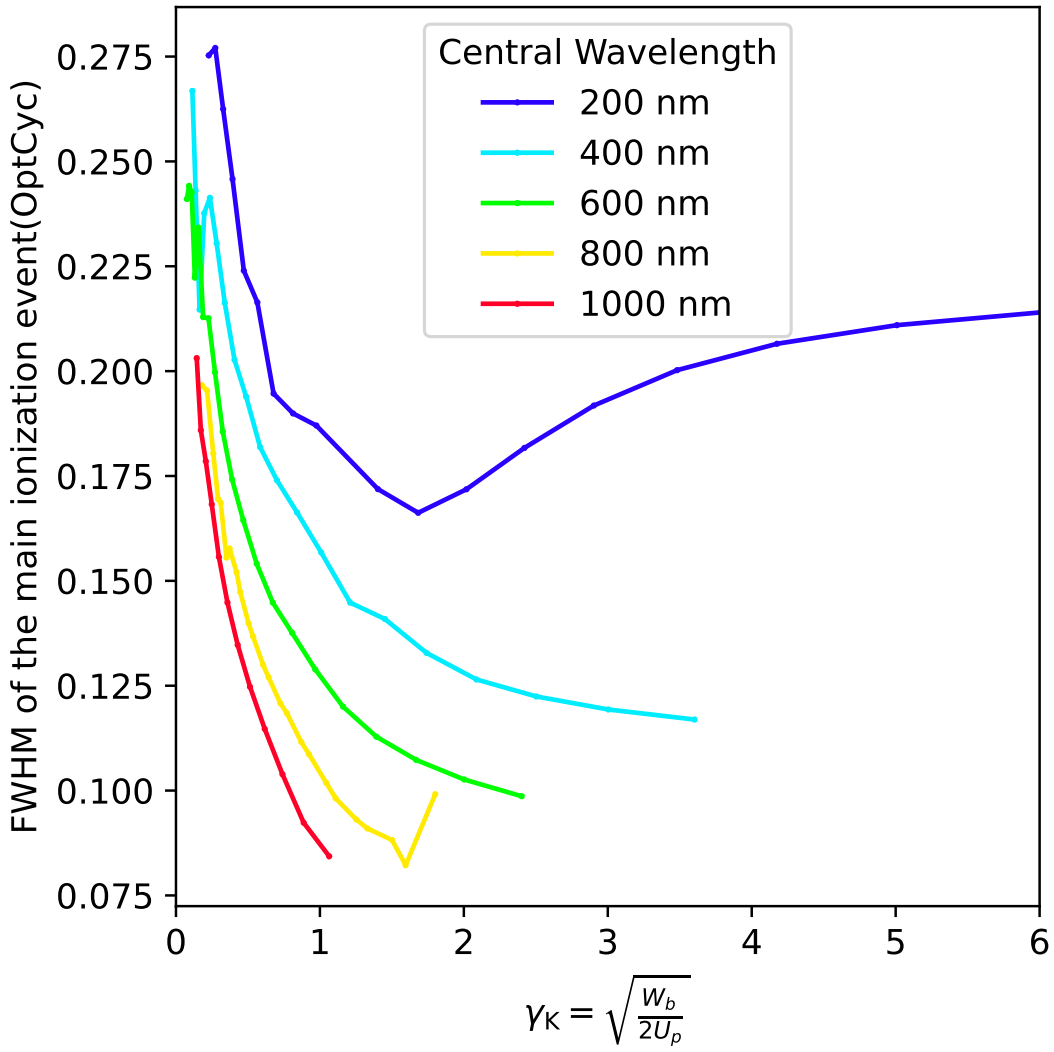

Figure 12.13.: Like Figure 12.12, a combined plot that summarizing the effect of tuning both the central wavelength and the intensity. The x axis is the same **Keldysh parameter**, but the y axis is the FWHM of the central ionization event in **optical cycles**, i.e., normalized for the fact that the duration of a pulse's cycle increases with its wavelength. It was shown in Figure 12.12 that shorter wavelengths allow shorter ionization duration in absolute terms. However, relative to the duration of the entire pulse, longer wavelength pulses can limit the ionization events to a much smaller portion within its optical cycle. This is due to the increased nonlinearity of the interaction.

13. Concluding Remarks

I achieved the initial stated purpose of laying an analytical, quantum mechanical, ab initio foundation for photoconductive sampling. Comparison of the classical notion of photoconductive sampling with the analytical approach leads to an important conclusion. Using ionization rate models to describe strong-field light-matter interaction is a classical interpretation of an inherently quantum mechanical process. However, in photoconductive sampling, the gating function, which is a quantum mechanical quantity, when interpreted classically, is the ionization rate. Thus, for all setups measuring a free charge's momentum or energy like in photoconductive sampling, one may define the ionization rate in an unambiguous manner as the gating function. Ionization rate models do work for photoconductive sampling to a limited extent, and the gating function is an improvement over the existing ionization rates valid in a broader context.

The gating function answers the following question: "Given an optical field interacting with a medium, how much drift current would be observable if another field were switched on perpendicular to it?" This completely avoids dealing with the dubious discussion about when a bound electron is defined to become free in the presence of a strong field. The gating function quantifies the fundamental process of ionization caused by strong optical fields. Since the definition relies on the mathematical concept of gating rather than a physical model, it can be defined unambiguously within different frameworks. It may help comparing different analytical approaches on an equal footing.

From the LPS results, the main conclusion was the following: ionization rate is directly proportional to the instantaneous intensity of the pulse envelope. That was expected but the surprising part was the existence of additional fast oscillations that only disappeared once the rotating-wave approximation was made. Within the constraint of LPS, these oscillations will be unobservable, but if the gating function indeed can quantify ionization process even outside the context of photoconductive sampling, it hints at new physics.

NPS results were even more exciting. The apparent involvement of bound states at low light pulse intensities is remarkably interesting as, so far, very few studies have discussed this effect. Simply by existing, these states modify the drift current. While there still are other candidates to rule out, I hope that the results from my toy models lay a convincing argument to inspire further investigation into the bound

states.
The most important conclusion from NPS was the insight gained into the relationship between the central wavelength of the pulse, its intensity, and the duration for which the electron gets ionized. It has very direct and practical consequences. Any technique aiming to exploit nonlinear light-matter-interaction for attosecond metrology will benefit from the knowledge that there is an ideal range of intensity and wavelength that minimizes the photoionization duration. At first, simply increasing the intensity to be deep in the tunneling regime sounds enticing. The ionization will be a function of the instantaneous field intensity and instantaneous response should result in better time resolutions. My results suggest quite the contrary. Based on the limitations placed by the experimental signal to noise ratio, reducing the intensity is better up-to the point where the participation of multi-photon ionization processes results in diminishing returns. In fact, for shorter wavelengths, SFA seems to suggest that this ideal intensity range lies at point where the Keldysh parameter is far greater than one.

List of Figures

Bibliography

1. Pukhov, A. Strong field interaction of laser radiation. *Reports on progress in Physics* **66,** 47 (2002).
2. Herbst, A., Scheffter, K., Bidhendi, M. M., Kieker, M., Srivastava, A. & Fattahi, H. Recent advances in petahertz electric field sampling. *Journal of Physics B: Atomic, Molecular and Optical Physics* (2022).
3. Reiss, H. R. in *Progress in Ultrafast Intense Laser Science III* 1–31 (Springer, 2008).
4. Lombardi, M. *et al.* The accuracy & stability of quartz watches. *Horological Journal* **150,** 57 (2008).
5. Laplante, P. A. *Comprehensive Dictionary of Electrical Engineering* - ISBN: 978-1-420-03780-7 (CRC Press, Boca Raton, Fla, 2018).
6. Schötz, J., Wang, Z., Pisanty, E., Lewenstein, M., Kling, M. F. & Ciappina, M. Perspective on petahertz electronics and attosecond nanoscopy. *ACS photonics* **6,** 3057–3069 (2019).
7. Hentschel, M., Kienberger, R., Spielmann, C., Reider, G. A., Milosevic, N., Brabec, T., Corkum, P., Heinzmann, U., Drescher, M. & Krausz, F. Attosecond metrology. *Nature* **414,** 509–513. ISSN: 1476-4687 (Nov. 2001).
8. Itatani, J., Quéré, F., Yudin, G. L., Ivanov, M. Y., Krausz, F. & Corkum, P. B. Attosecond streak camera. *Physical review letters* **88,** 173903 (2002).
9. Kienberger, R., Goulielmakis, E., Uiberacker, M., Baltuska, A., Yakovlev, V., Bammer, F., Scrinzi, A., Westerwalbesloh, T., Kleineberg, U., Heinzmann, U., *et al.* Atomic transient recorder. *Nature* **427,** 817–821 (2004).
10. Park, S. B., Kim, K., Cho, W., Hwang, S. I., Ivanov, I., Nam, C. H. & Kim, K. T. Direct sampling of a light wave in air. *Optica* **5,** 402–408 (2018).
11. Shin, J., Ivanov, I., Cho, W., Shrestha, R. & Kim, K. Temporal characterization of a two-color laser field using tunneling ionization. *Optics Express* **30,** 28686–28695 (2022).

12. Hwang, S. I., Park, S. B., Mun, J., Cho, W., Nam, C. H. & Kim, K. T. Generation of a single-cycle pulse using a two-stage compressor and its temporal characterization using a tunnelling ionization method. *Scientific reports* **9,** 1–6 (2019).

13. Keiber, S., Sederberg, S., Schwarz, A., Trubetskov, M., Pervak, V., Krausz, F. & Karpowicz, N. Electro-optic sampling of near-infrared waveforms. *Nature Photonics* **10,** 159–162 (2016).

14. Wu, Q. & Zhang, X.-C. Free-space electro-optic sampling of terahertz beams. *Applied Physics Letters* **67,** 3523–3525 (1995).

15. Kubullek, M., Wang, Z., von der Brelje, K., Zimin, D., Rosenberger, P., Schötz, J., Neuhaus, M., Sederberg, S., Staudte, A., Karpowicz, N., *et al.* Single-shot carrier–envelope-phase measurement in ambient air. *Optica* **7,** 35–39 (2020).

16. Zimin, D., Weidman, M., Schötz, J., Kling, M. F., Yakovlev, V. S., Krausz, F. & Karpowicz, N. Petahertz-scale nonlinear photoconductive sampling in air. *Optica* **8,** 586–590 (May 2021).

17. Korobenko, A., Johnston, K., Kubullek, M., Arissian, L., Dube, Z., Wang, T., Kübel, M., Naumov, A. Y., Villeneuve, D., Kling, M. F., *et al.* Femtosecond streaking in ambient air. *Optica* **7,** 1372–1376 (2020).

18. Pearsall, T. P. *Quantum Photonics* - ISBN: 978-3-319-55144-9 (Springer, Berlin, Heidelberg, 2017).

19. Keldysh, L. *et al.* Ionization in the field of a strong electromagnetic wave. *Sov. Phys. JETP* **20,** 1307–1314 (1965).

20. Ammosov, M. V., Delone, N. B. & Krainov, V. P. *Tunnel ionization of complex atoms and atomic ions in electromagnetic field* in *High intensity laser processes* **664** (1986), 138–141.

21. Bauer, D. & Mulser, P. Exact field ionization rates in the barrier-suppression regime from numerical time-dependent Schrödinger-equation calculations. *Physical Review A* **59,** 569 (1999).

22. Scrinzi, A. Ionization of multielectron atoms by strong static electric fields. *Physical Review A* **61,** 041402 (2000).

23. Faisal, F. H. Multiple absorption of laser photons by atoms. *Journal of Physics B: Atomic and Molecular Physics (1968-1987)* **6,** L89 (1973).

24. Maxwell, J. C. *A dynamical theory of the electromagnetic field* (Wipf and Stock Publishers, 1996).

25. Jackson, J. D. & Okun, L. B. Historical roots of gauge invariance. *Reviews of Modern Physics* **73,** 663 (2001).

26. Barth, I. & Lasser, C. Trigonometric pulse envelopes for laser-induced quantum dynamics. *Journal of Physics B: Atomic, Molecular and Optical Physics* **42,** 235101 (Nov. 2009).
27. Wallace, W., Kielpinski, D., Litvinyuk, I. & Sang, R. Precise calibration of few-cycle laser pulses with atomic hydrogen. *Journal of Physics B: Atomic, Molecular and Optical Physics* **50** (Dec. 2017).
28. Zheltikov, A. Keldysh parameter, photoionization adiabaticity, and the tunneling time. *Physical Review A* **94,** 043412 (2016).
29. Lifshitz, E., LD & (JB), S. L. *Quantum Mechanics; Non-relativistic Theory* (Pergamon Press New York, 1965).
30. Boca, M. On the properties of the Volkov solutions of the Klein–Gordon equation. *Journal of Physics A: Mathematical and Theoretical* **44,** 445303 (2011).
31. Reiss, H. Theoretical methods in quantum optics: S-matrix and Keldysh techniques for strong-field processes. *Progress in Quantum Electronics* **16,** 1–71. ISSN: 0079-6727 (1992).
32. Ivanov, M. Y., Spanner, M. & Smirnova, O. Anatomy of strong field ionization. *Journal of Modern Optics* **52,** 165–184 (2005).
33. Condon, E. U. & Shortley, G. H. in *The theory of Atomic Spectra* 114–118 (Cambridge U.P., 2004).
34. Kohn, W. & Sham, L. J. Self-consistent equations including exchange and correlation effects. *Physical review* **140,** A1133 (1965).
35. Halliday, D., Resnick, R. & Walker, J. *Fundamentals of physics* (John Wiley & Sons, 2013).
36. Auston, D. H. Picosecond optoelectronic switching and gating in silicon. *Applied Physics Letters* **26,** 101–103 (1975).
37. Waynant, R. W. & Ediger, M. N. *Electro-optics handbook* (Citeseer, 2000).
38. Wilson, J. & Hawkes, J. F. Optoelectronics-an introduction. *Optoelectronics-An introduction (2nd edition* (1989).
39. Marks, R. J. I. *Introduction to Shannon sampling and interpolation theory* (Springer Science & Business Media, 2012).
40. Corkum, P. B. Plasma perspective on strong field multiphoton ionization. *Phys. Rev. Lett.* **71,** 1994–1997 (13 Sept. 1993).
41. Krausz, F. & Ivanov, M. Attosecond physics. *Rev. Mod. Phys.* **81,** 163–234 (1 Feb. 2009).

42. Schiffrin, A., Paasch-Colberg, T., Karpowicz, N., Apalkov, V., Gerster, D., Mühlbrandt, S., Korbman, M., Reichert, J., Schultze, M., Holzner, S., Barth, J. V., Kienberger, R., Ernstorfer, R., Yakovlev, V. S., Stockman, M. I. & Krausz, F. Optical-field-induced current in dielectrics. *Nature* **493,** 70–74. ISSN: 1476-4687 (Jan. 2013).

43. Schötz, J., Maliakkal, A., Blöchl, J., Zimin, D., Wang, Z., Rosenberger, P., Alharbi, M., Azzeer, A. M., Weidman, M., Yakovlev, V. S., *et al.* The emergence of macroscopic currents in photoconductive sampling of optical fields. *Nature communications* **13,** 1–10 (2022).

44. Sederberg, S., Zimin, D., Keiber, S., Siegrist, F., Wismer, M. S., Yakovlev, V. S., Floss, I., Lemell, C., Burgdörfer, J., Schultze, M., Krausz, F. & Karpowicz, N. Attosecond optoelectronic field measurement in solids. *Nature Communications* **11,** 430. ISSN: 2041-1723 (Jan. 2020).

45. Ossiander, M., Golyari, K., Scharl, K., Lehnert, L., Siegrist, F., Bürger, J., Zimin, D., Gessner, J., Weidman, M., Floss, I., *et al.* The speed limit of optoelectronics. *Nature communications* **13,** 1–8 (2022).

46. Arons, A. B. & Peppard, M. Einstein's Proposal of the Photon Concept—a Translation of the Annalen der Physik Paper of 1905. *American Journal of Physics* **33,** 367–374 (1965).

47. Krausz, F. From femtochemistry to attophysics. *Physics World* **14,** 41 (2001).

48. Lewenstein, M., Balcou, P., Ivanov, M. Y., L'huillier, A. & Corkum, P. B. Theory of high-harmonic generation by low-frequency laser fields. *Physical Review A* **49,** 2117 (1994).

49. Gagnon, J., Goulielmakis, E. & Yakovlev, V. S. The accurate FROG characterization of attosecond pulses from streaking measurements. *Applied Physics B* **92,** 25–32 (2008).

50. Keathley, P. D., Bhardwaj, S., Moses, J., Laurent, G. & Kaertner, F. X. Volkov transform generalized projection algorithm for attosecond pulse characterization. *New Journal of Physics* **18,** 073009 (2016).

51. Cho, W., Shin, J.-u. & Kim, K. T. Reconstruction algorithm for tunneling ionization with a perturbation for the time-domain observation of an electric-field. *Scientific Reports* **11,** 1–9 (2021).

52. Scrinzi, A. tRecX—An environment for solving time-dependent Schrödinger-like problems. *Computer Physics Communications* **270,** 108146 (2022).

53. Scrinzi, A. Infinite-range exterior complex scaling as a perfect absorber in time-dependent problems. *Phys. Rev. A* **81,** 053845 (5 May 2010).

54. He, F., Ruiz, C. & Becker, A. Absorbing boundaries in numerical solutions of the time-dependent Schrödinger equation on a grid using exterior complex scaling. *Physical Review A* **75,** 053407 (2007).

55. Tao, L. & Scrinzi, A. Photo-electron momentum spectra from minimal volumes: the time-dependent surface flux method. *New Journal of Physics* **14,** 013021 (Jan. 2012).

56. Morales, F., Bredtmann, T. & Patchkovskii, S. iSURF: a family of infinite-time surface flux methods. *Journal of Physics B: Atomic, Molecular and Optical Physics* **49,** 245001 (Nov. 2016).

57. Cuyt, A. in *Handbook of continued fractions for special functions* 344 (Springer, 2008).

58. Virtanen, P., Gommers, R., Oliphant, T. E., Haberland, M., Reddy, T., Cournapeau, D., Burovski, E., Peterson, P., Weckesser, W., Bright, J., van der Walt, S. J., Brett, M., Wilson, J., Millman, K. J., Mayorov, N., Nelson, A. R. J., Jones, E., Kern, R., Larson, E., Carey, C. J., Polat, İ., Feng, Y., Moore, E. W., VanderPlas, J., Laxalde, D., Perktold, J., Cimrman, R., Henriksen, I., Quintero, E. A., Harris, C. R., Archibald, A. M., Ribeiro, A. H., Pedregosa, F., van Mulbregt, P. & SciPy 1.0 Contributors. SciPy 1.0: Fundamental Algorithms for Scientific Computing in Python. *Nature Methods* **17,** 261–272 (2020).

59. Reiss, H. R. Limits on Tunneling Theories of Strong-Field Ionization. *Phys. Rev. Lett.* **101,** 043002 (4 July 2008).

60. Sarachik, E. S. & Schappert, G. T. Classical Theory of the Scattering of Intense Laser Radiation by Free Electrons. *Phys. Rev. D* **1,** 2738–2753 (10 May 1970).

61. Celnikier, L. M. in. Chap. Section 1: Environment, Chapter 4: Trajectories (Atlantica Séguier Frontières, 1993).

62. Ohgoda, S., Tolstikhin, O. I. & Morishita, T. Photoionization of hydrogen in a strong static electric field. *Phys. Rev. A* **95,** 043417 (4 Apr. 2017).

63. Arbó, D., Tőkési, K. & Miraglia, J. E. Limitations of the strong field approximation in ionization of the hydrogen atom by ultrashort pulses. *The European Physical Journal D* **51,** 303–312 (2009).

64. Wu, Y. & Yang, X. Strong-coupling theory of periodically driven two-level systems. *Physical review letters* **98,** 013601 (2007).

65. Fewell, M. P. Adiabatic elimination, the rotating-wave approximation and two-photon transitions. *Optics communications* **253,** 125–137 (2005).

66. Prepelitsa, O. Multiphoton resonant ionization of a hydrogen-like atom by a strong electromagnetic field. *Optics and Spectroscopy* **89,** 327–333 (2000).

67. Volkova, E., Popov, A. & Tikhonova, O. Resonant multiphoton ionization of the 1s state of a hydrogen atom in a strong laser field. *Optics and Spectroscopy* **88,** 1–6 (2000).